I. INTRODUCTION

II. BEAM PROPERTIES

III. OSCILLATION PHYSICS

A. Theoretical framework

B. Where will we be in 5-10 years ?

C. Detector considerations

We would like to measure the oscillation probabilities $P(\nu_\alpha \to \nu_\beta)$ as a function of the baseline L and neutrino energy E (and hence L/E) for all possible initial and final flavors α and β. This requires a beam with a well known initial flavor content, and a detector that can identify the flavor of the interacting neutrino. The neutrinos interact in the detector via charged current (CC) and neutral current (NC) interactions to produce a lepton accompanied by a hadronic shower arising from the remenants of the struck nucleon. In CC interactions the final state lepton tags the flavor (β) of the interacting neutrino.

At a neutrino factory in which, for example, positive muons are stored, the initial beam consists of 50% ν_e and 50% $\overline{\nu}_\mu$. In the absense of oscillations, the ν_e CC interactions produce electrons and the $\overline{\nu}_\mu$ CC interactions produce positive muons. Note that the charge of the final state lepton tags the flavor (α) of the initial neutrino or antineutrino. In the presence of $\nu_e \to \nu_\mu$ oscillations the ν_μ CC interactions produce negative muons (i.e. wrong–sign muons). Similarly, $\overline{\nu}_\mu \to \overline{\nu}_e$ oscillations produce wrong–sign electrons, $\overline{\nu}_\mu \to \overline{\nu}_\tau$ oscillations produce events tagged by a τ^+ and $\nu_e \to \nu_\tau$ oscillations produce events tagged by a τ^-. Hence, there is a variety of information that can be used to measure or constrain neutrino oscillations at a neutrino factory, namely the rates and energy distributions of events tagged by (a) right–sign muons, (b) wrong–sign muons, (c) electrons or positrons (their charge is difficult to determine in a massive detector), (d) positive τ–leptons, (e) negative τ–leptons, and (f) no charged lepton. If these measurements are made when there are alternately positive and negative muons decaying in the storage ring, there are a total of 12 spectra that can be used to extract information about the oscillations. Some examples of the predicted measured spectra are shown as a function of the oscillation parameters in Figs. 1 and 2 for a 10 kt detector sited 7400 km downstream of a 30 GeV neutrino factory. Clearly, the high intensity ν_e, $\overline{\nu}_e$, ν_μ, and $\overline{\nu}_\mu$ beams at a neutrino factory would provide a wealth of precision oscillation data.

FIGURES

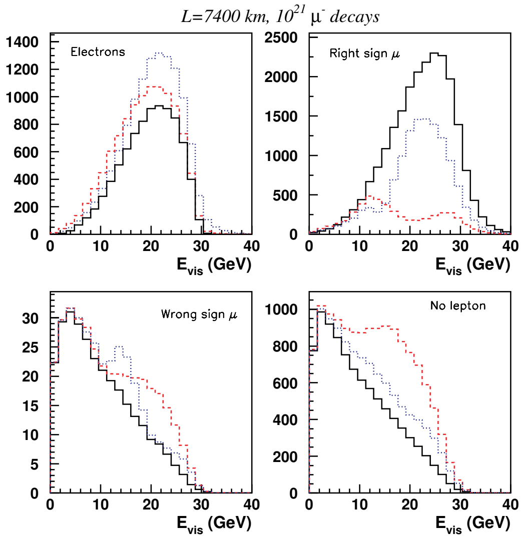

FIG. 1. Visible energy spectra for four event classes when $10^{21}\mu^-$ decay in a 30 GeV neutrino factory at $L = 7400$ km. Three cases are considered. Black histogram: no oscillations. Blue dotted histogram: $\delta m^2_{32} = 3.5\times10^{-3}$ eV^2/c^4, $\sin^2\theta_{23} = 1$. Red dashed histogram: $\delta m^2_{32} = 7\times10^{-3}$ eV^2/c^4, $\sin^2\theta_{23} = 1$. The distributions are for an ICANOE-type detector, and are from Ref. xxx.

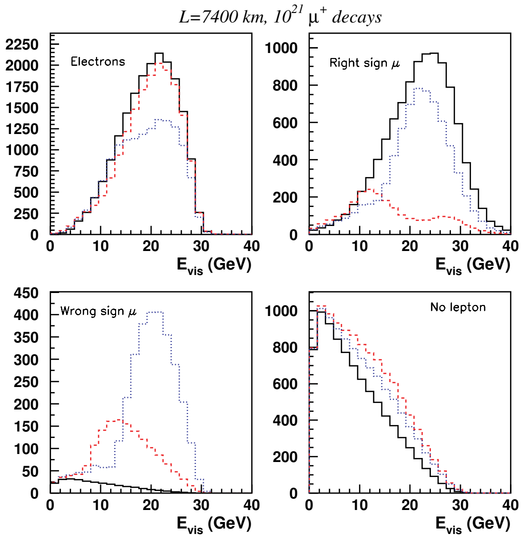

FIG. 2. Same as previous figure, but with positive muons circulating in the storage ring. The difference between the two figures is due to the different cross section for neutrinos and antineutrinos, and to matter effects.

The detectors required at a neutrino factory will have many similarities to the detectors that have been designed for the next generation of experiments at conventional neutrino beams. However, there are some important differences. First, we can anticipate more massive detectors. The sensitivity of a neutrino factory oscillation experiment is proportional to the product of the detector mass and beam intensity. It is likely that the cost of increasing the MINOS detector fiducial mass (for example) by a factor of a few is smaller than the cost of increasing the neutrino factory beam intensity by a factor of a few. Therefore, we believe that it is reasonable to assume that detectors at a neutrino factory would be a factor of a few to a factor of 10 more massive than the generation of neutrino detectors presently under construction. Second, the presence of both neutrinos and antineutrinos in the same beam at a neutrino factory places a premium on measuring the sign of the charge of the lepton produced in CC interactions. Charge–sign determination may not be practical for electrons, but is manditory for muons and highly desirable for τ–leptons. Finally, a relatively low energy threshold for the detection and measurement of wrong–sign muons is very desirable. This is because high muon detection thresholds require high energy interacting neutrinos, and hence a high energy neutrino factory. Since the muon acceleration system at a neutrino factory is likely to be expensive, low energies are preferable.

In the following sections we begin by considering general detector issues for the measurement of final state muons and τ–leptons, and then consider some specific candidate neutrino factory detectors. Some of these detector applications are quite new and are just beginning to be studied; for the more mature detectors the "neutrino" energy resolution, the signal efficiency, background rejection, and fiducial mass are discussed.

1. Muon identification and measurement

The detection and measurement of muons (especially those of opposite sign to the muons in the storage ring) is crucial for many of the key oscillation physics measurements at a neutrino factory. Before considering some specific neutrino factory detectors it is useful to condisider more generally muon backgrounds and related issues. Background muons can be produced in NC and CC interactions by:

(i) Pions or kaons from the hadronic shower that decay to produce a muon.

(ii) Non-interacting pions which fake a muon signature (punch-through).

(iii) Charm meson production and muonic decay.

A background muon event can be produced when a background "muon" of the appropriate sign is recorded in (a) a NC event or (b) a CC event in which the primary lepton has been lost. If the background muon hass the same charge–sign as that in the storage ring the resulting event will be a background for disappearance measurements, but more imporantly, if it has the opposite sign then the event will be a background for wrong–sign muon appearance measurements.

The integrated wrong-sign background is shown in Fig. 3 as a function of the minimum muon energy accepted for Steel/Scintillator and water detectors downstream of 20 GeV and 50 GeV neutrino factories. The charm background comes from ν_μ CC events where the primary muon was less than XX GeV. The peak at low muon energies is from the hadron shower itself and from punch through, while the long tail is from shower particles decaying to muons.

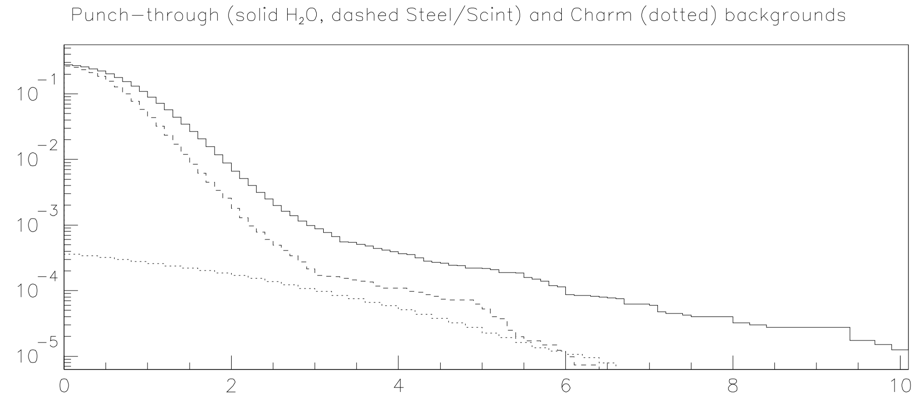

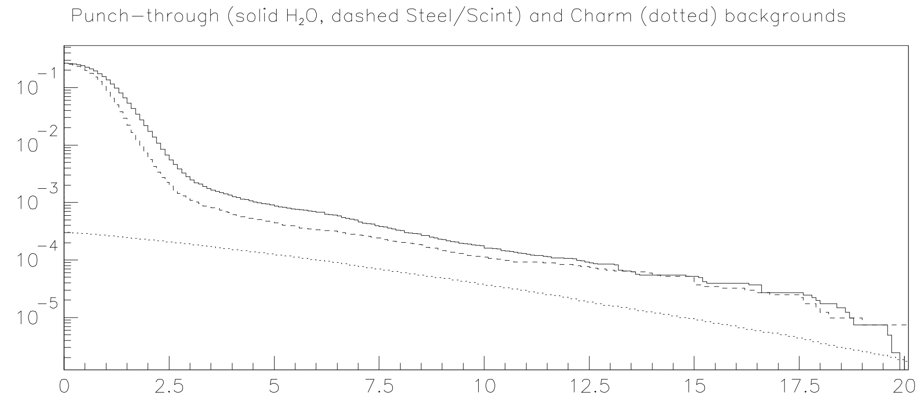

FIG. 3. Background levels from punch through, pion/kaon decay, and charm backgrounds for a 20GeV ring (left) and a 50GeV ring (right)

In general there are two different standards for background levels which are relevant: that of a disappearance experiment and that of an appearance experiment. Background estimates are not trivial, but if the backgrounds for a disappearance measurement are at the one per cent level, then the uncertainties on those backgrounds can be expected to be small compared to the flux uncertainty. On the other hand, wrong-sign muon appearance measurement uncertainties are expected to be dominated by the statistics. So an extremely agressive background level requirement would be to have less than of the order of one background event. If there are several thousand charged current events expected, then this would require a 10^{-4} to 10^{-5} background rejection.

Backgrounds can be suppressed by imposing a minimum energy requirement on the measured muon. Figure 4 shows the effect of several different minimum muon energy cuts on a simulated oscillation signal observed in a steel-scintillator type detector at a 20 GeV muon storage ring, at a baseline length of 2800km [2]. A muon threshold energy of 4 GeV for example depletes the low energy part of observed measured "neutrino energy" distribution, degrading but not completely removing the information about the neutrino oscillation parameters that is encoded in the shape of the distribution. A 4 GeV threshold at a 20 GeV neutrino factory is probably tolerable. If higher thresholds are needed to reject backgrounds, then a higher energy neutrino factory is desirable. If a lower energy neutrino factory is to be viable, then lower muon thresholds are desirable.

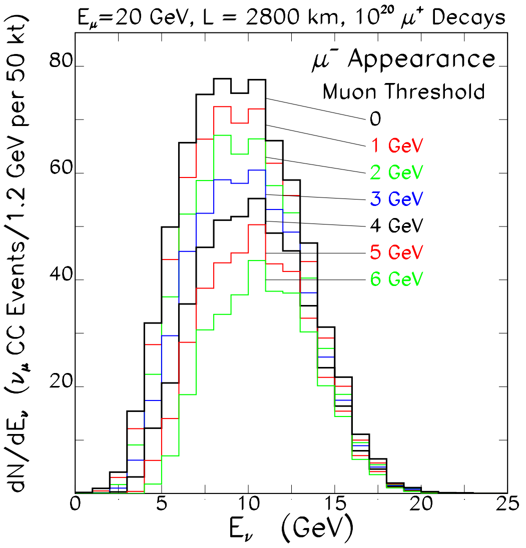

FIG. 4. Reconstructed neutrino energy distribution for several different minimum muon energy cuts for a 20GeV ring

SAY SOMETHING HERE ABOUT BACKGROUND LEVELS IN WATER AND IRON WITH A 4 GEV THRESHOLD, AND FURTHER POSSIBLE WAYS TO REDUCE BACKGROUNDS AT THE EXPENSE OF EFFICIENCY.

2. τ–lepton identification and measurement

Because the tau decays to a muon 17% of the time, it is the second easiest lepton whose charge can be identified: the idea is to have part of the detector sensitive to the missing momentum in a tau to mu decay, followed by a muon spectrometer. We discuss briefly three detectors which in theory should be able to do tau charge identification, but in reality cannot be made on as large a scale as the muon-id detectors. By the time a muon storage ring begins to send a beam to a far detector, it is assumed that tau appearance will have been demonstrated by the CERN to Gran-Sasso experiments. If there are no surprises in the τ appearance measrements, and if LSND is not confirmed, tau appearance will not be a high priority at the muon storage ring experiment, but still desirable since the objective is to map the entire leptonic mixing matrix. If there is a sterile neutrino sector, it is imperative that we be able to measure as many neutrino transitions as possible, not simply $\nu_\mu \to \nu_\mu$ and $\nu_e \to \nu_\mu$.

3. A magnetized Steel/Scintillator detector

Steel/Scintillator calorimeters have been used extensively in past neutrino experiments, so their performance is well understood, documented, and simulated. We take advantage of that experience in this study.

In the most general case, such a detector consists of iron plates interspersed with scintillator planes; the scintillator could be segmented transversely, or a separate detector system (i.e. drift chambers) could be used in order to provide transverse position measurement. For any resonable transverse segmentation, the transverse resolution is dominated by multiple coulomb scattering (MCS), and the momentum resolution for muon reconstruction depends on the amount of MCS and the magnitude of the integral Bdl traversed by any given track.

The neutrino interactions in such a detector have a well defined topology. Neutral current (NC) interactions of all flavors consist of a hadronic shower reconstructed as a large energy deposition in a small number of scintillator units. $\nu_\mu(\bar{\nu_\mu})$ CC interactions which have a muon in the final state, are characterized by a long pentrating track in addition to the hadronic shower. For $\nu_e(\bar{\nu_e})$ CC interactions, the electron in the final state cannot be resolved, so the events look similar to NC interactions. The same topology characterizes the $\nu_\tau(\bar{\nu_\tau})$ CC interactions, unless the τ decays with a μ in the final state. The above picture gets modified, if the detector resolution and specific cases in the evolution of the hadron shower are considered. The first consideration comes from the finite ability of the detector to resolve muons from the hadron shower in CC interactions. Muons which don't penetrate for a long enough distance past the hadron-shower-end cannot be reconstructed, thus imposing a minimum length (energy) cuttof for the muon, above which a CC event can be identified. The peaking behavior at a few GeV in figure 3 is dominated by the "length" of hadronic showers for both 20 and 50 GeV rings. The second consideration comes from the possibility of reconstructing as primary muons non-prompt muons or punchthrough pions in NC-like events ($\nu_m u$ NC, all ν_e, and most ν_τ). The sources of these muons were listed in section III C 1.

The experimental technique proposed for this study is the observation of "wrong-sign" muons. Given the above discussion, the issues which we need to address in order to understand the sensitivity of the magentized Fe/Sci detector are: the efficiency to identify and measure the charge of the primary muon (from the leptonic vertex) and the efficiency to remove secondary muons (from the hadronic vertex) without eliminating the signal.

For the present study, we considered a detector geometry similar to the CCFR/NuTeV calorimeter [6], with the addition of a toroidal field of 1T. One module of this detector is shown in figure III C 3. For a 0.7 kTon detector, 42 modules of cross section $3m \times 3m$ were used. The ultimate cross section of one unit of this type of detector will likely be determined by the largest size over which one can generate a large magnetic field. The detector performance, however, depends primarily on the longitudinal segmentation of small sections of the detector. The segmentation needs to be fine enough to measure that a muon has left the region of the hadronic shower, and once the segmentation is that fine then the momentum resolution of that final state muon is simply determined by the magnetic field of the steel and the thickness of the plates.

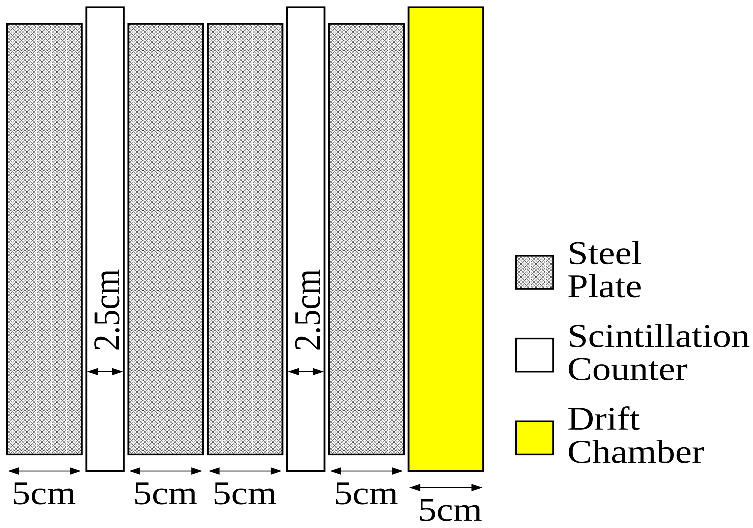

FIG. 5. CCFR/NuTeV calorimeter module

For the simulations, we used the parameterized Monte Carlo developed by the NuTeV collaboration [7], modified to include particle tracing in the magnetic field added in the calorimeter. The hadron energy resolution of this detector is described in detail in [6], and is approximately $\delta E_{had} = \frac{0.85}{\sqrt{E_{had}}}$. The momentum resolution depended on the path length of the track in the steel, and on the containment of the muon in the detector. For muons which ranged out in the detector the effective momentum resolution was $\delta P/P = 5\%$, while for tracks which left the fiducial volume of the detector the resolution depended on the usual $\frac{\theta_{MCS}}{\theta_{BdL}} \sim \frac{\delta P}{P}$ relation. The simulation included a detailed parameterization of the hadron-shower development, with the inclusion of charm production and π, κ decays (the data set on which the decay probability parameterization was tuned included muons with momentum higher than 4GeV); π punchthrough was not included in the parameterization.

In order to be conservative, and in order to eliminate possible bias from the specifics of the Monte Carlo used (π, κ decay parameterization limit and no π punchthrough), all muons with generated energy below 4GeV are considered lost. The pattern recognition and charge-identification efficiency is considered to be 100% for muons with generated energy greater than 4GeV and path length in steel greater than 50cm past the end of the hadron shower. For the background events, we considered all the π, κ decay events with the "wrong charge" in NC interactions, and all the charm production events and π, κ decay events in CC where the primary muon was considered lost according to the length and energy requirement described above, while the secondary muon was found with the "wrong charge".

To reduce the above backgrounds, we cut on the transverse component of the muon momentum relative to the hadron shower direction (P_t). Since the muons for background events originate in the shower, the relative transverse momentum is expected to be smaller than that for muons from the leptonic vertex. In figure 6 the reconstructed P_t^2 distribution is shown for both signal and background muons in the case of a 20 GeV $\mu+$ staorage ring, with oscillation parameters taken from the theory scenario IA (reference theory section here).

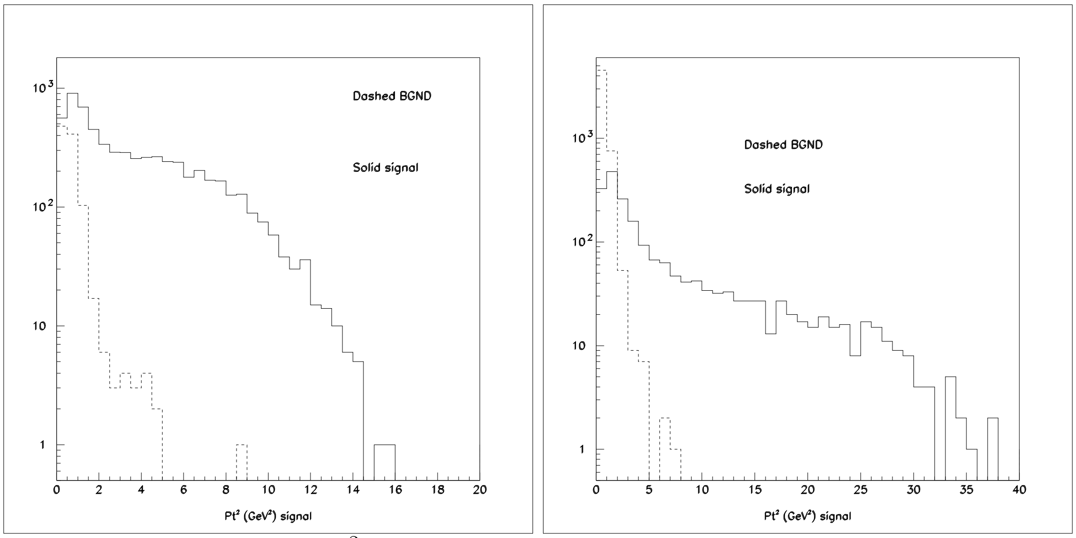

FIG. 6. Reconstructed μ P_t^2 with respect to the shower direction for 20 GeV and 50 GeV $\mu+$ rings.

We investigated the performance of the detector in the case of scenario 1 oscillation parameters, and for a baseline of 2800km. The input neutrino beams tested were from both 50GeV and 20GeV muon storage rings. The event rates were normalized to a fine-grained detector with a fiducial mass of 10kt and a storage ring with 10^{20} stored muons per charge per year. The reconstructed wrong-sign muon spectrum for the case of a 20GeV storage ring with a $\mu+$ beam is shown in figure III C 3. The top plot shows the signal from $\nu_e \rightarrow \nu_\mu$ and $\nu_e \rightarrow \nu_\tau \rightarrow \mu + X$ events, and the potential background distribution as a function of the muon momentum. The bottom plot shows the same distributions after the pattern recognition and background rejection cuts (described above) were applied.

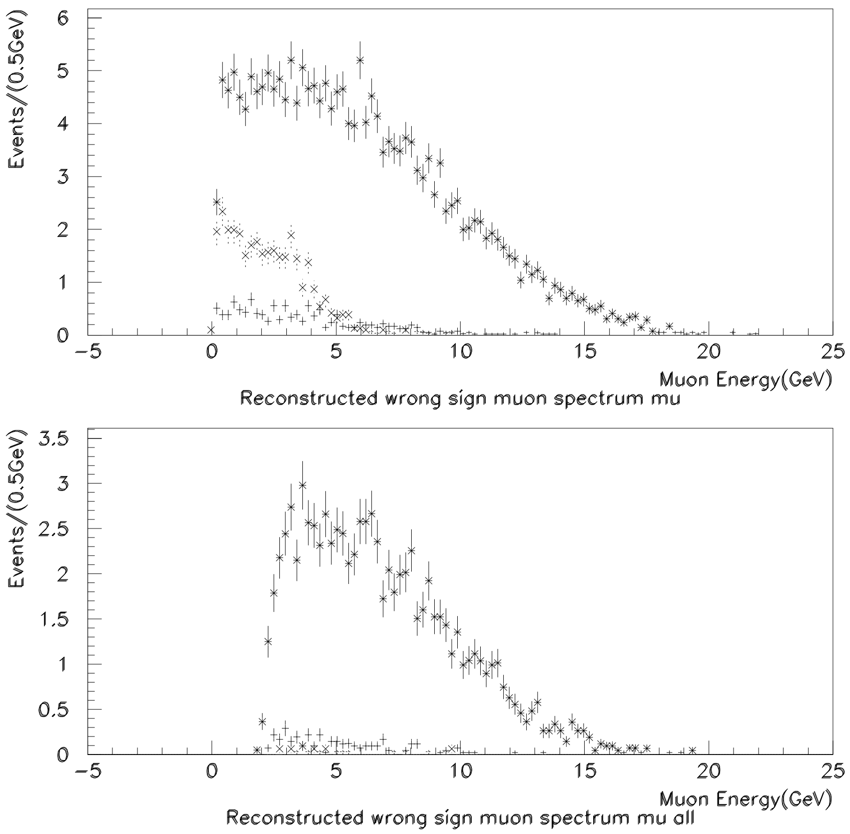

FIG. 7. Reconstructed wrong-sign muons as a function of the muon energy for a $\mu+$ 20 GeV ring. Top plot accepted events for the signal ($\nu_e \to \nu_\mu$–stars– and $\nu_e \to \nu_\tau \to \mu + X$–crosses) and the potential backgrouns (x). The bottom plot shows the signal and the background after cuts.

The summary of the studies appears in table I, but one can clearly see from figure III C 3 that the signal to background with a coarse-grained detector is very high in scenario 1.

TABLES

TABLE I. Wrong-sign muon rates after all cuts for a 10kTon steel-scintillator detector with 10^{20} muon decays, and scenario IA as proposed in the theory section.

μ Ring Energy (GeV)	Charge	$\nu_e \to \nu_\mu$ events	$\nu_e \to \nu_\tau \to \mu + X$ events	background events	efficiency (signal)	purity (background)
50	+	268.5	15.4	21.6	0.50±0.02	0.013±0.006
50	-	55.2	4.7	3.5	0.48±0.02	0.006±0.008
20	+	85.7	3.5	0.7	0.41±0.02	0.021±0.008

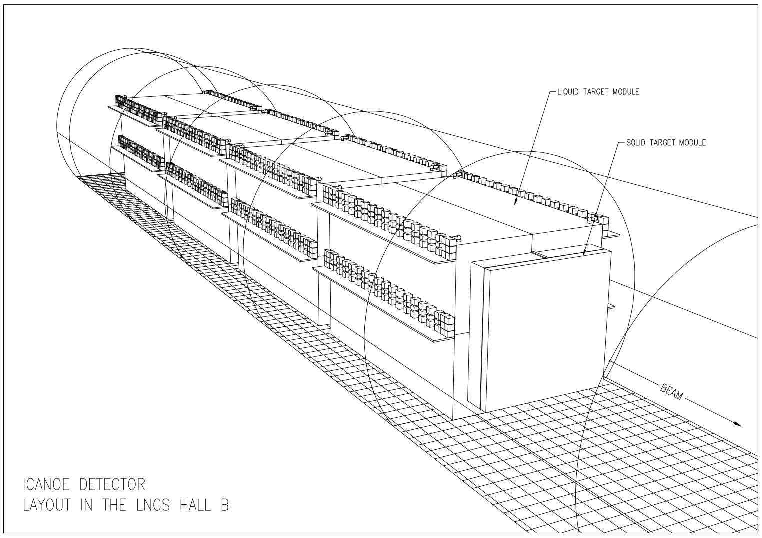

FIG. 8. Perspective view of the Liquid Argon TPC detector with 4 supermodules.

The neutrino factory studies that were done on a Liquid Argon TPC were performed using the ICANOE monte carlo. One ICANOE detector unit consists of a liquid argon TPC followed by a magnetic spectrometer where the muon charge is measured. The layout is shown in figure 8.

The Liquid Argon TPC has extremely fine granularity, which makes it very similar in strategy to a bubble chamber. It is instrumented with 3mm pitch wires which allow tracking, dE/dx measurements, electromagnetic, and hadronic calorimetery. Electrons and photons can be identified event by event, and their energies are measured with a resolution $5\%/\sqrt{E}$. The hadron energy resolution is $20\%/\sqrt{E}$. The magnetic spectrometer is needed to measure the muon energy and charge, but to maintain a good level of acceptance it is assumed that it will be also instrumented in such a way as to allow the hadron energy of showers which leak into the calorimeter to be correctly (albeit with worse resolution) measured. The muon momentum resolution is expected to be 20%.

In the design used in these studies, the liquid Argon module is 18m deep with a cross section of $11.3m \times 11.3m$. The active (total) mass of one Liquid Argon module is 1.4 kton (1.9 kton). The magnetized calorimeter module is 2.6m deep with a cross section of $9m \times 9m$, and represents 0.8 kton. It consists of 2 m of steel, corresponding to 7.4 λ_{int} and 59 X_0 interleaved with a total of 0.6 m of tracking chambers. Four SuperModules with a total length of the experiment of 82.5 m and a total active mass of 9.3 kton fully instrumented are being considered for the baseline option.

ICANOE can fully reconstruct neutrino (and antineutrino) events of all active flavors, and with an energy ranging from the tens of MeV to the tens of GeV, for the relevant physics analyses. The unique imaging capabilities of the liquid argon TPC allow one to cleanly determine whether a given event is a nu_μ charged current event, a ν_e charged current event, or a neutral current event. The addition of the spectrometer allows $\nu_\mu/\overline{\nu}_\mu$ discrimination.

In order to make the most out of the muon spectrometer it is assumed that it will be instrumented to work as a calorimeter as well.

For the studies presented in the next section, the ICANOE fast simulation was used. Neutrino interaction events are generated, with a proper treatment of quasi-elastic interactions, resonance and deep-inelastic processes. The 4-vectors for all the particles generated smeared, according to the resolutions derived from the full simulation. Muonic decays of pions and kaons are also considered, for a proper wrong- and right-sign muon background treatment. The sensitivity to oscillation parameters is impressive and is given in detail in the Oscillation Measurements section.

5. A Water Cerenkov detector

Preliminary studies have explored the possibility of using a large water Cherenkov detector as a distant target for a neutrino factory beam. Traditionally this type of detector has been used for measuring much lower energy neutrinos than what will be produced at a muon storage ring, but to date water cerenkov neutrino detectors are the only existing neutrino detectors with masses already in the 50kton range. Water is of course the lightest target material under consideration in this report, but this type of detector has several advantages when extrapolating to large masses. The primary advantages of such a detector are the low cost of the target material, the need to instrument only the surface of a very large volume, and good calorimetry. A large volume guarantees containment of hadronic and electromagnetic showers (as well as muons up to a certain energy). The low density of the target and good angular resolution from the cerenkov cone could mean that the overall hadron angle resolution could be at least as good as that coming from steel-scintillator calorimeters but probably even better.

Water Cherekov devices as large as 50kton (Super-Kamiokande) are already in operation and may continue data-taking for ten years or more. Therefore, the response of the existing Super-K detector at a distance of 9100 km has been studied as a test case. Next generation detectors, up to 1 Mton in mass, are technically feasible and are currently under consideration for proton decay and neutrino measurements, sited perhaps at the Kamioka mine or elsewhere. The low density of the target and good angular resolution from the cerenkov cone could mean that the overall hadron angle resolution could be at least as good as that coming from steel-scintillator calorimeters but probably even better.

For this study, the primary question is the suitability of a water Cherenkov detector for the higher energy neutrino beam produced by a 10-50 GeV muon storage ring. At these energies, the multiplicity of hadrons is greater than for typical atmospheric neutrino interactions, and event topologies are correspondingly more complex. Software adapted from the Super-Kamiokande experiment has been used to study the detector response to neutrinos from 10 GeV and 50 GeV muon storage rings. It is worth noting that neutrinos produced by a 50 GeV muon beam induce a large number of events in the material (rock) surrounding any detector (producing an entering muon), and for a Super-Kamiokande sized device these events actually outnumber the those produced in the detector's water volume itself. Both contained and entering events have therefore been studied.

The response of a detector the size of Super-K changes drastically as a function of beam energy. At 10 GeV muon energy, 57current events are fully contained in the inner water volume, whereas only 11exists for events containing penetrating muons; at 10 GeV (50 GeV) both $\bar{\nu}_e$ and neutral current events are contained greater than 98(90algorithm works produces a reasonably pure (89fully contained events in the 10 GeV beam, but e-like events are a mixture of of $\bar{\nu}_e$-CC, NC and ν_μ-CC contamination. Exiting and entering events are pure samples of ν_μ-CC simply by their penetrating nature. The muon angular resolution (xx°) is much less than the muon-neutrino angular correlation (xx°). With 2×10^20 decays of a 50 GeV beam and a baseline of 9100 km, approximately $200,000$ ν_μ charged current events would be observed entering or exiting the current Super-K detector. Combined with muon charge identification this sample should be able to provide good oscillation measurements.

In order to be useful in a neutrino beam created by decaying muons, however, charge identification is required. Two possibilities have been proposed: the first, in which there are several large water targets, each one followed by a thin muon spectrometer, and the second, in which a magnetic field is introduced into the water volume itself. Although the first design would have lower geometrical acceptance and a higher muon energy threshold, it would pose much less of a problem for the phototubes since the magnetic field would presumably be well-contained in the spectrometer. The second proposal could in principle have good low energy muon momentum acceptance, but the resolution on the muon and hadron shower angles might be compromised.

For a field internal to the target, a 0.5-1 kG field is sufficient to visually determine the charge of a several meter-long ($> 1GeV$) muon, but no automated algorithms have yet been developed. A number of conceptual magnet designs have been studied: solenoidal, toroidal, and concentric current loops in the center or at the ends of the detector. A detailed study of one particular design has shown that one can immerse the central volume of a Super-Kamiokande sized detector in a 0.5 kG magnetic field while leaving only a 0.5G fringe field (which may be acceptable with shielding and/or local compensation) in the region of the PMTs. Many of the difficulties inherent in placing a field inside a water detector would be avoided if an alternative light collector (insensitive to the field) were used. Work on magnet design and alternative light collection is ongoing, but the internal magnetic field option must be considered speculative at this point.

The results we will report on in the remainder of this section are for a water cerenkov detector with an external magnetic field, because neutrino event reconstruction is more s-traightforward to simulate and the spectrometer technology are all well-understood and used already. Although the studies on this detector are far more preliminary than those listed above, they are included here because they look promising and warrant further investigation. The results presented below are from a LUND/GEANT monte carlo which uses as its geometry a 40mx40mx100m box of water, followed by a 1m long muon spectrometer. This simulation can be used to study acceptance issues and background contamination for a range of geometries and storage ring energies. The background levels for this type of detector compared to that of steel-scintillator detectors are discussed above.

Figure III C 5 shows the geometric acceptance for the box-like water cerenkov detector as a function of distance of the neutrino interaction vertex from the spectrometer, for charged current ν_μ events from 20 and 50GeV storage ring energies. The loss in acceptance close to the spectrometer is due to rejection of events where there is more than one muon which traverses the spectrometer (where the extra muon comes from background processes). It is clear that for a 20GeV muon storage ring one would want a muon spectrometer much more frequently than once every 100m. Of course, the smaller the ratio of water thickness to steel thickness the more it approximates a magnetized steel/scintillator target interspersed with water volumes with fine graularity. (remember steel has a density of 8 times that of water!).

FIG. 9. Acceptance in a water target for charged current ν_μ and $\overline{\nu}_\mu$ events in a 20 and 50 GeV storage ring, as a function of distance of the neutrino interaction vertex from the muon spectrometer.

Clearly more work is needed to optimize this kind of detector, but it might be a inexpensive compromise between a coarse-grained sampling calorimeter and a very fine-grained liquid argon TPC.

6. Specialized τ–lepton detectors

1. PerfluoroHexane

A Cerenkov detector filled with perfluorohexane (C6F14) has been proposed by Roger Forty to be used in the CERN to Gran Sasso beamline to look for tau appearance [1]. The geometry of the detector is that there are several volumes of the target, followed by short muon spectrometer slices. The density of C6F14 is 1.7 times that of water, and a 1Ton detector of a very different geometry already exists at DELPHI. The way a tau would appear in this detector is that a few cerenkov photons would be emitted by the tau as it traverses the C6F14, and then the muon would emit many more cernkov photons resulting in a circle at the phototube window with an offset center. This technique would probably not work for high hadron energy showers, however, because of the large number of charged particles that would result in overlaping rings near the initial tau ring anyway. Figure 10 shows a quasi-elastic ν_τ event (no hadron energy) from this kind of detector, complete with two rings.

2. Emulsion

One category of new detectors uses thin ($\sim 100\mu m$) sheets of emulsion combined with low-density ($\sim 300\mu m$) spacers, so that one can measure kinks that occur when a tau decays by comparing the slope of a track before and after the spacer [3]. This would be very useful for identifying taus and electrons. For charge identification one could put the detector volume in a large magnetic field, like the ones currently being built for LHC experiments. Then one could measure the curvature of the electron, tau, or muon track in the spacer volume where there would be no smearing due to multiple scattering. In that case, the charge measurement would be limited by the angular resolution of the emulsion. For an emulsion angular resolution of 2mrad, for a 10GeV charged particle one could achieve a 5σ charge determination with simply a $2Tesla$ field, and a $1.2mm$ spacer volume [4]. As very rough guess as to the scale of such a device, consider a detector which consists of 1kton of Steel in 1mm thin sheets, and an equal volume of thin sheets of emulsion plus low density spacers: that device could measure roughly $3 \times (5m)^3$ (since one kTon of steel is roughly $(5m)^3$). The ATLAS barrel toroidal magnet system covers approximately $7600m^3$, with a field that varies from 4.2Tesla at a radius of 9.5m and a field of about 2.4Tesla at a radius of 19.5m [5].

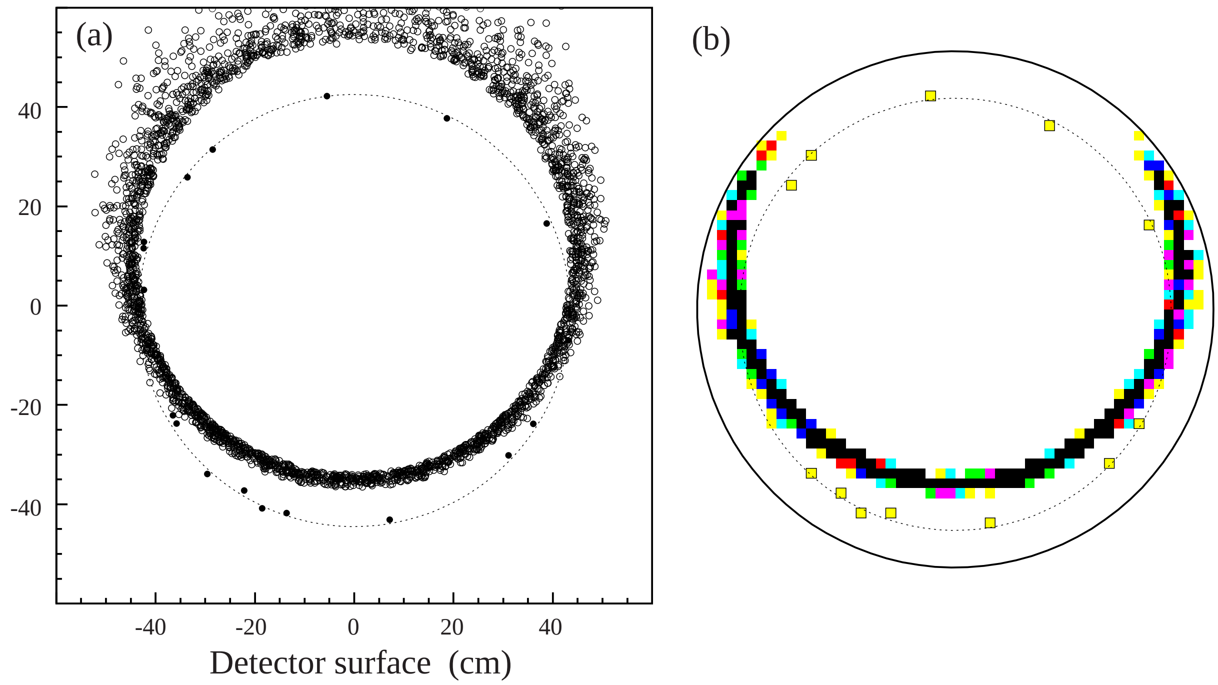

FIG. 10. Quasielastic ν_τ event in a perfluoroHexane cerenkov detector: the ring described by about eight hits on the left is from the tau before it decays.

3. Kinematic Reconstruction Detectors

One type of detector which is sensitive to tau decays on a statistical level (although not event-by event) can be labeled kinematic reconstruction detectors. These are very fine grained detectors so on average some acoplanarity is seen in the tau decays. If one has a low-Z, less dense target material in the presence of a magnetic field, there is a longer path-length to measure the electron's charge. Another advantage of low-Z materials is that the nuclear interaction length per g/cm^2 is shorter, so it may be easier to distinguish muons from pions. Disadvantages include distinguishing pions from electrons, and poorer jet energy resolution.

Consider a target whose active element is Micro-Strip Gas Chambers (MSGC) with 50 μm space resolution. We assume we need a sagitta of 100 μm for 50 GeV electrons traveling for 1 radiation length. This leads to the following constraint:

$$\text{sagitta}(\mu\text{m}) = \frac{3.75\ B(\text{T})\ X_0^2(\text{cm})}{p(\text{GeV})} \tag{1}$$

The cost of a superconducting solenoid magnet scales as:

$$\text{Cost}(\text{M\$}) \approx 0.523 E^{2/3}(\text{MJ}) \tag{2}$$

where E is the stored magnetic energy:

$$E = (\pi/2\mu_0) B^2 R^2 L \tag{3}$$

Putting these equations together we find

$$\text{Cost} \propto B. \tag{4}$$

Thus, we want to minimize B, which corresponds to maximizing X_0 for a given target mass. We could choose for example nylon, which has a long radiation for a given mass, 42 g/cm^2, and a low density, giving a radiation length of 37 cm. Then, we would need a B field of 1 T. If we then placed MSGC every 10 cm, we would need 10,000 m^2 of MSGC per kiloton of target material. The magnet for this experiment would have roughly the volume of the magnet for the CMS experiment at LHC. However, it would have a field of 1 T instead of 4 T, so the cost would be reduced by a factor of 6.

It may be more economical to use drift chambers instead of MSGC. The NOMAD neutrino experiment has operated drift chamber planes with an impressive resolution of 150 μm. If we followed this drift chamber design, we find from Eq. 1 that we would need to increase the spacing between tracking planes by a factor of 1.7. This would increase the cost of the magnet by 45%. If we further followed the NOMAD design, for which most of the target mass consists of drift chambers, the total volume would increase by an factor of 10, but the magnetic field would only need to be 300 Gauss.

7. Detector summary

In this section we have described a variety of different detection techniques for an oscillation experiment, each with its own advantages and disadvantages. For scenario IA from the theory section both a Liquid Argon TPC and a Steel/Scintillator calorimeter are adequate for reducing the backgrounds and seeing the oscillation signal at many sigma, as long as the energy in the muon storage ring is above 20GeV. Details on the precision of each kind of detector's measurement are given in the next section. As was stated at the beginning of this section, the critical aspects of a detector are the following: signal efficiency, background rejection, neutrino energy resolution, and ultimate detector mass.

There are two kinds of detector geometries that are being considered: one where the neutrino target itself is magnetized, and one where the target is not magnetized but is follwed by a thin spectrometer to measure the charge of the muon. In the first case one has only coarse readout segmentation in the neutrino interaction region; in the second case there is detailed event-by-event information at the neutrino vertex. Consequently, it is not a surprise that the fine-grained detector can make more efficient cuts to reduce backgrounds, and will have more precise event by event "neutrino" energy resolution. However, the signal efficiency from geometric effects is different between the two detectors, as is the ultimate detector mass.

A detector that has a target followed by a muon spectrometer is limited by the muon energy required to reach and traverse the spectrometer, which is where its charge is measured. It will be important to optimize the spacing between successive target and spectrometer modules. Also, in order to get this fine segmentation the target density is lower (Liquid Argon has a density of $1.4 g/cm^3$, while the Steel/Scintillator detector has an average density of $4 g/cm^3$), which for a given underground cavern volume means that the overall mass of a steel/scintillator detector will be larger.

The question of whether or not a given detector can survive at the surface of the earth has not been quantitatively studied for a steel scintillator detector. From past experience however it is expected that for muon storage rings above 20GeV a steel scintillator detector would work at ground level, although in that case one would likely be forced to only study events with a muon in the final state.

One important aspect to remember is that neutrino beams are not attenuated, and therefore one could imagine pointing a beam to an underground location with a fine-grained neutrino detector filling the cavern, but then just downstream of that location, where the neutrino beam crosses the surface of the earth, one could also place a steel scintillator detector. In this way one could make many cross checks of oscillations by looking at both neutral and charged current events in the fine-grained detector, yet in the same beam get the very high fiducial mass that is needed to do precision studies of wrong-sign muons.

Characteristic	Steel/Scint	Liquid Argon TPC
Resolutions of: Electron Energy	$50\%/\sqrt{E}$	$3\%/\sqrt{E} \oplus 1\%$
Hadron Energy	$85\%/\sqrt{E}$	$20\%/\sqrt{E} \oplus 5\%$
Muon Energy	5%	20%

Hadron Shower Angle		$.02 \oplus .21/\sqrt{p} rad$ (each hadron)
P_t^2 resolution		
Muon Angle	5 to 7% for 50cm to 100cm path length	
Maximum ktonnage	50 kton	30 kton
What limits size?		safety, tunnel
Charge MIS-ID probability		
Minimum earth coverage needed	0 m **	50 m
Fiducial Acceptance expected		
Background rejection cuts considered	$P_\mu > 2GeV$ $P_t^2 > 4GeV^2$	$P_\mu > 2GeV$
Signal acceptance from these cuts	50	$> 99\%$
Background level	get from pgs table	2×10^{-5}
Maximum B field	1T	2 T
Transverse segmentation		3 mm wire pitch

TABLE II. ** The overburden required for a steel-scintillator calorimeter depends on the energy of the muon storage ring; but in the past this type of detector has been used with minimal contamination in the ν_μ charged current sample above a neutrino energy of 5GeV at ground level.

D. Oscillation measurements

The pattern of neutrino masses, the neutrino oscillation scheme, and the associated leptonic mixing matrix can be determined at a neutrino factory by measuring the rates and energy distributions of events tagged by (a) right–sign muons, (b) wrong–sign muons, (c) electrons, (d) tau–leptons, and (e) the absence of a charged lepton. If these measurements are made when there are alternately positive and negative muons decaying in the storage ring, there are a total of 10 spectra that can be used to extract information about the oscillations. Some examples of the predicted measured spectra are shown as a function of the oscillation parameters in Figs. 1 and 2 for a 10 kt detector sited 7400 km downstream of a 30 GeV neutrino factory. The spectra are normalized to correspond to 10^{21} muon decays in the beam–forming straight section. Clearly, the high intensity ν_e, $\overline{\nu}_e$, ν_μ, and $\overline{\nu}_\mu$ beams at a neutrino factory would provide a wealth of precision oscillation data.

In the following sub-sections the oscillation measurements that can be made at a neutrino factory are discussed as a function of baseline, muon beam energy, and muon beam intensity. In particular we consider the first observation of $\nu_e \to \nu_\mu$ oscillations, the measurement of the sign of δm^2 and hence the pattern of neutrino masses, the first observation of $\nu_e \to \nu_\tau$ oscillations, the measurement of $\nu_\mu \to \nu_\tau$ oscillations, precisions measurements of the oscillation parameters, and the search for CP violation in the lepton sector. These results are based on the calculations described in more detail in Refs. [9,**?**,**?**,**?**].

1. Observation of $\nu_e \to \nu_\mu$ oscillations and the pattern of neutrino masses

At a neutrino factory $\nu_e \to \nu_\mu$ oscillations would be signaled by the appearance of CC interactions tagged by a wrong–sign muon. Within the framework of three–flavor oscillations the $\nu_e \to \nu_\mu$ oscillation amplitude is approximately proportional to $\sin^2 2\theta_{13}$. At the present time only an upper limit exists on $\sin^2 2\theta_{13}$. The next generation long-baseline oscillation experiments are expected to be able to improve the sensitivity to $\sin^2\theta_{13} \approx 10^{-2}$, i.e. about one order of magnitude below the present bound. If $\sin^2 2\theta_{13}$ is in this range we would expect to observe $\nu_e \to \nu_\mu$ oscillations at a relatively low intensity neutrino factory, measure matter effects, and determine the pattern of neutrino masses. This is discussed further in the remainder of this sub–section.

It is useful to define the $\sin^2 2\theta_{13}$ "reach" for an experiment as the value of $\sin^2 2\theta_{13}$ for which a given physics goal would be met. We take as our initial goal the observation of 10 $\nu_e \to \nu_\mu$ events tagged by a wrong–sign muon. Consider first the $\sin^2 2\theta_{13}$ reach for a 50 kt detector sited a distance L from a 20 GeV neutrino factory in which there are $10^{19}\mu^+$ decays in the beam–forming straight section. The baseline–dependent $\sin^2 2\theta_{13}$ reach is shown in Fig. 11 for a three-flavor oscillation scenario in which $\delta m^2_{21}, \sin^2 2\theta_{12}$, and $\sin^2 2\theta_{23}$ correspond to the LAM scenario IA1, and the value of δm^2_{32} is varied over the favored SuperK range. If δm^2_{32} is in the center of the SuperK range, the $\sin^2 2\theta_{13}$ reach is about an order of magnitude below the currently excluded region, improving slowly with decreasing L. The reach improves (degrades) by a about a factor of 2 (3) if δm^2_{32} is at the upper (lower) end of the current SuperK range. If the oscillation parameters correspond to the LAM scenario IA1 ($\sin^2 2\theta_{13} = 0.04$), then only 2×10^{18} muon decays are required at a 20 GeV neutrino factory to observe 10 signal events in a 50 kt detector at $L = 2800$ km. The calculation assumes that CC events producing muons with energy less than (greater than) 4 GeV are detected with an efficiency of 0 (1). The number of muon decays needed to observe 10 $\nu_e \to \nu_\mu$ events is shown in Fig. 12 as a function of E_μ for the LAM scenario IA1, the SAM scenario IA2, and the LOW scenario IA3. The required muon beam intensities decrease with increasing E_μ, and are approximately proportional to $E_\mu^{-1.6}$. Compared with the SAM and LOW scenarios, slightly less intensity is needed for the LAM scenario, showing the small but finite contribution to the signal rate from the sub–leading δm^2 scale. In all three scenarios (LAM, SAM, LOW) a 20 GeV neutrino factory providing 10^{19} decays in the beam–forming straight section would enable the first observation of $\nu_e \to \nu_\mu$ oscillations in a 50 kt detector provided $\sin^2 2\theta_{13} > 0.01$.

Having established $\nu_e \to \nu_\mu$ oscillations, further data taking would facilitate the measurement of matter effects and the determination of the sign of δm^2, and hence the pattern of neutrino masses. To illustrate the effect of matter on the $\nu_e \to \nu_\mu$ oscillation probability, the predicted measured energy distributions 2800 km downstream of a 30 GeV neutrino factory are shown in Figs. 13 and 14 for respectively $\nu_e \to \nu_\mu$ and $\overline{\nu}_e \to \overline{\nu}_\mu$ wrong–sign muon events. The distributions are shown for a range of positive and negative values of δm^2_{32}. Note that for a given $|\delta m^2_{32}|$, if $\delta m^2_{32} < 0$ we would expect to observe a lower wrong–sign muon event rate and a harder associated spectrum when positive muons are stored in the neutrino factory than when negative muons are stored. On the other hand, if $\delta m^2_{32} > 0$ we would expect to observe a higher wrong–sign muon event rate and a softer associated spectrum when positive muons are stored in the neutrino factory than when negative muons are stored. Hence, measuring the differential spectra when positive and negative muons are alternately stored in the neutrino factory can enable the sign of δm^2_{32} to be unambiguously determined.

The expected number of wrong–sign muon events are listed in Table III for the LAM scenario IA1, and a 50 kt detector downstream of a neutrino factory providing $10^{19}\mu^+$ decays and the same number of μ^- decays. The event rates are shown for both signs of δm^2_{32}, and for various storage ring energies and baselines. Even at a 20 GeV neutrino factory the signal rates at $L = 7332$ and 2800 km are large enough to permit the sign of $\delta m^2_{32} > 0$ to be determined with a few years of data taking.

We conclude that for the LAM, SAM, and LOW three–flavor mixing scenarios we have considered a 20 GeV neutrino factory providing 10^{19} decays in the beam–forming straight section would be a viable entry–level facility. In particular, with a 50 kt detector and a few years of data taking either $\nu_e \to \nu_\mu$ oscillations would be observed and the sign of δm^2_{32} determined or a very stringent upper limit on $\sin^2 2\theta_{13}$ will have been obtained (discussed later). Long baselines (> 2000 km) are preferred. The longest baseline we have considered (7332 km) has the advantage of lower total event rates and hence lower background rates.

2. Observation of $\nu_e \to \nu_\tau$ oscillations

We begin by considering the LAM scenario IA1, and ask: What beam intensity is needed to make the first observation of $\nu_e \to \nu_\tau$ oscillations in a detector that is 2800 km downstream of a 20 GeV neutrino factory ? The $\nu_e \to \nu_\tau$ and the accompanying $\overline{\nu}_\mu \to \overline{\nu}_\tau$ event rates are shown in Fig. 15 as a function of the oscillation parameters $\sin^2 2\theta_{13}$ and δm^2_{32}. The $\nu_e \to \nu_\tau$ signal rate is sensitive to both of these parameters, and hence provides an important consistency check for three-flavor mixing: the observation or non–observation of a $\nu_e \to \nu_\tau$ signal must be consistent with the oscillation parameters measured from, for example, $\nu_e \to \nu_\mu$, $\nu_\mu \to \nu_\tau$, and ν_μ disappearance measurements. For the LAM scenario IA1 the observation of 10 signal events in a 5 kt detector (with 100% τ–lepton efficiency) would require $7 \times 10^{19} \mu^+$ decays in the beam forming straight section. Very similar beam intensities are required for the SAM and LOW scenarios (IA2 and IA3). Note that, over the $\sin^2 2\theta_{13}$ range shown in Fig. 15, the $\overline{\nu}_\mu \to \overline{\nu}_\tau$ rates are one to two orders of magnitude higher than the $\nu_e \to \nu_\tau$ rates. Hence, we will need a detector that can determine the sign of the tau–lepton charge at the $2\sigma - 3\sigma$ level, or better.

Let us define the $\sin^2 2\theta_{13}$ "reach" for an experiment as the value of $\sin^2 2\theta_{13}$ for which we would observe 10 $\nu_e \to \nu_\tau$ events when there are 10^{20} muon decays in the beam–forming straight section of a neutrino factory. The $\sin^2 2\theta_{13}$ reach is shown as a function of the baseline and storage ring energy in Fig. 16 for a 5 ky detector and an oscillation scenario in which all of the parameters except $\sin^2 2\theta_{13}$ correspond to scenario IA1. The reach improves with energy (approximately $\sim E^{-1.6}$) and is almost independent of baseline except for the highest energies and baselines considered. We conclude that within the LAM, SAM, and LOW scenarios, a 20 GeV storage ring in which there are $O(10^{20})$ muon decays per year would begin to permit an observation of, or meaningful limits on, $\nu_e \to \nu_\tau$ oscillations provided a multi-kt detector with good tau–lepton identification and charge discrimination is practical.

Next, consider the oscillation scenarios IB1 (atmospheric + LSND scales) and IC1 (three–flavor with atmospheric, solar, and LSND data stretched). In these cases the leading δm^2 is large (0.3 $\mathrm{eV}^2/\mathrm{c}^4$) and medium baseline experiments (L = 10-100 km) become interesting. As an example, consider a medium baseline experiment a few $\times 10$ km downstream of a 20 GeV neutrino factory in which there are $10^{20} \mu^+$ decays. The $\nu_e \to \nu_\tau$ and accompanying $\overline{\nu}_\mu \to \overline{\nu}_\tau$ event rates are shown in Fig. 17 as a function of the baseline and the phase δ with the other oscillation parameters corresponding to scenario IB1. In contrast to the $\overline{\nu}_\mu \to \overline{\nu}_\tau$ rates, the $\nu_e \to \nu_\tau$ rates are very sensitive to δ, and for $|\delta| > 20^\circ$ can be very large, yielding thousands of events per year in a 1 kt detector at $L = 60$ km, for example. Note that the corresponding $\overline{\nu}_\mu \to \overline{\nu}_\tau$ rate is of order 100 events. For small $|\delta|$ the $\overline{\nu}_\mu \to \overline{\nu}_\tau$ rate will dominate the τ appearance event sample. For larger $|\delta|$ the $\nu_e \to \nu_\tau$ rate dominates. Good τ charge determination will therefore be important to measure both $\nu_e \to \nu_\tau$ and $\overline{\nu}_\mu \to \overline{\nu}_\tau$ oscillations.

Now consider the τ appearance rates in scenario IC1. In this case the rates are not sensitive to δ and, for a 1 kt detector at $L = 60$ km, there are about 8000 $\nu_e \to \nu_\tau$ events and 93000 $\overline{\nu}_\mu \to \overline{\nu}_\tau$ events. A detector with 3σ (or better) τ-lepton charge discrimination would enable these two rates to be separately measured.

We conclude that measurements of the $\nu_e \to \nu_\tau$ oscillation rate at a neutrino factory would provide an important test of the oscillation scenario. In LAM, SAM, and LOW three-flavor oscillation scenarios a 20 GeV neutrino factory providing $O(10^{20})$ muon decays could permit an observation of, or meaningful limits on, $\nu_e \to \nu_\tau$ oscillations. In LSND-type scenarios where the leading δm^2 scale is large, a 20 GeV neutrino factory providing $O(10^{19})$ muon decays might already permit hundreds of $\nu_e \to \nu_\tau$ events to be measured. It should be noted that the feasibility of a multi-kt detector with good τ identification and charge sign determination has not been explored in detail at this stage, and further work is required to identify the best detector technology for this, and determine the expected resolutions and efficiencies.

3. Measurement of $\nu_\mu \to \nu_\tau$ oscillations

The present SuperK data suggests that the atmospheric neutrino deficit is due to $\nu_\mu \to \nu_\tau$ oscillations. If this is correct the next generation of accelerator based long baseline experiments are expected to measure these oscillations. Hence $\nu_\mu \to \nu_\tau$ appearance measurements at a neutrino factory are likely to be less interesting than $\nu_e \to \nu_\mu$ or $\nu_e \to \nu_\tau$ appearance measurements. Nevertheless, for a fixed neutrino factory energy and baseline, it is of interest to measure or put stringent constraints on all of the appearance channels so that the sum of the appearance modes can be compared with the disappearance measurements. Hence, we briefly consider $\nu_\mu \to \nu_\tau$ rates at a neutrino factory. Note that at a 20 GeV neutrino factory the average interacting neutrino energy is of order 15 GeV, and for δm^2 within the favored SuperK range, the first oscillation maximum occurs at baselines of 7000 ± 3000 km. At shorter baselines the oscillation probabilities are lower and hence the signal/background ratio is lower, although the signal rate can be higher.

Consider first a 5 kt detector 2800 km downstream of a 20 GeV neutrino factory in which there are 10^{20} muon decays. The $\overline{\nu}_\mu \to \overline{\nu}_\tau$ event rates are shown in Fig. 15 as a function of the $\sin^2 2\theta_{13}$ and δm^2_{32}, with the other oscillation parameters corresponding to the LAM scenario IA1. If negative muons are stored in the neutrino factory, the resulting $\nu_\mu \to \nu_\tau$ event rates would be about a factor of two higher than the $\overline{\nu}_\mu \to \overline{\nu}_\tau$ rates shown in the figure. A neutrino factory providing $\mathrm{O}(10^{20})$ muon decays would enable $\nu_\mu \to \nu_\tau$ appearance data samples of a few hundred to a few thousand events to be obtained. Similar rates are expected in SAM and LOW three-flavor mixing scenarios.

Next consider a longer baseline example in which a 10 kt ICANOE–type detector is 7400 km downstream of a 30 GeV neutrino factory which provides 10^{20} muon decays in the beam forming straight section. The main advantage of a longer baseline is that the total interaction rate, and hence the τ–lepton background, is reduced. The energy distribution for events in which there is no charged lepton can directly reflect the presence of a ν_τ signal (see Fig. 1). The non–τ events in this event sample can be suppressed using topology–dependent kinematic cuts. It is desirable that the τ charge–sign also be determined which, with an external muon spectrometer, will be possible for the $\tau \to \mu$ subsample. We conclude that the measurement of $\nu_\mu \to \nu_\tau$ oscillations with high statistical precision will be possible at a neutrino factory in long and very long baseline experiments. A more complete study is warranted.

4. Determination of $\sin^2 2\theta_{13}$, $\sin^2 2\theta_{23}$, and δm^2_{32}

Consider first the determination of $\sin^2 2\theta_{13}$. The most sensitive way to measure $\sin^2 2\theta_{13}$ at a neutrino factory is to measure the $\nu_e \to \nu_\mu$ oscillation amplitude, which is approximately proportional to $\sin^2 2\theta_{13}$. More explicitly, the value of $\sin^2 2\theta_{13}$ is extracted from a fit to the spectrum of CC interactions tagged by a wrong–sign muon. Background contributions from, for example, muonic decays of charged mesons must be kept small, which favors small total event samples and hence long baselines.

As an example, consider a 10 kt ICANOE–like detector that is 7400 km downstream of a 30 GeV neutrino factory. The simulated energy spectrum of wrong-sign muon events is shown in Fig. 18 for three–flavor oscillations with the parameters $\delta m^2_{32} = 3.5 \times 10^{-3}$ eV^2/c^4, $\sin^2 2\theta_{23} = 1$, and $\sin^2 2\theta_{13} = 0.05$. Note that the backgrounds predominantly contribute to the low energy part of the spectrum. To fit the observed spectrum and extract $\sin^2 2\theta_{13}$ matter effects must be taken into account. The modification of the oscillation probability due to matter effects is a function of the profile of the matter density ρ between the neutrino source and the detector. The density profile is known from geophysical measurements, and this knowledge can either be used in the fit, or alternatively ρ can be left as a free parameter. It has been shown that both methods give consistent results [11], and that the uncertainties on the fitted values of ρ and $\sin^2 2\theta_{13}$ are not strongly correlated. However, the fitted value for $\sin^2 2\theta_{13}$ does depend on the assumed values for $\sin^2 \theta_{23}$ and δm^2_{32}. The measured right–sign muon (ν_μ disappearance) distribution, together with the distributions of events tagged by electrons, τ–leptons, or the absence of a lepton, can be used to constrain these additional oscillation parameters. Hence, the best way to extract $\sin^2 2\theta_{13}$ is from a global fit to all of the observed event distributions, with the oscillation parameters (and optionally ρ) left as free parameters. If the density profile is left as a free parameter, the fit determines its value with an uncertainty of about 10%. Examples of fit results in the ($\sin^2 2\theta_{13}$, $\sin^2 \theta_{23}$)–plane are shown in Fig. 19 for 10^{19}, 10^{20}, and 10^{21} muon decays in the neutrino factory. As the beam intensity increases the measurements become more precise. With $10^{19}\mu^+$ and μ^- decays $\sin^2 2\theta_{13}$ and $\sin^2 2\theta_{23}$ are determined with precisions of 38% and 20% respectively. With 10^{21} decays these precisions have improved to 4% and 5%. If the baseline is decreased from 7400 km to 2900 km the oscillation parameters are determined with comparable (although slightly worse) precisions (Fig. 20). We conclude that within the framework of three–flavor mixing, provided $\sin^2 2\theta_{13}$ is not too small, a global fit to the observed oscillation distributions would enable $\sin^2 2\theta_{13}$, $\sin^2 \theta_{23}$, and δm^2_{32} to be simultaneously determined.

To illustrate the ultimate sensitivity to the oscillation parameters that might be achievable at a high intensity neutrino factory, consider next a 40 kt Fe-scintillator detector downstream of a 50 GeV neutrino factory in which there are $10^{21}\mu^+$ decays followed by $10^{21}\mu^-$ decays. Fit results in the (matter density, $\sin^2 2\theta_{13}$)–plane are shown in Fig. 21 for three baselines. The precision on the $\sin^2 2\theta_{13}$ determination is a few percent. At the longest shortest baselines (732 km) matter effects are too small to obtain a good determination of the matter density parameter.

Consider next the precision with which the oscillation parameters can be determined if $\sin^2 2\theta_{13}$ is very small, and hence no $\nu_e \to \nu_\mu$ oscillation signal is observed. The resulting limits on $\sin^2 2\theta_{13}$ are shown as a function of δm^2_{32} in Fig. 22 for a 10 kt ICANOE type detector 7400 km downstream of a 30 GeV neutrino factory in which there are $10^{20}\mu^+$ decays followed by $10^{20}\mu^-$ decays. The resulting upper limit on $\sin^2 2\theta_{13}$ would be O($10^{-3} - 10^{-4}$), about three orders of magnitude below the present experimental bound, and 2 orders of magnitude below the bound that would be expected at the next generation of long–baseline experiments.

The limit would become even more stringent at a higher intensity neutrino factory. As an example of the ultimate sensitivity that might be achievable, in Fig. 23 the limits on $\sin^2 2\theta_{13}$ are shown as a function of δm^2_{32} and baseline for a 40 kt Fe-scintillator detector downstream of a 50 GeV neutrino factory in which there are $10^{21}\mu$ decays. The non–observation of $\nu_e \to \nu_\mu$ oscillations could result in an upper limit on $\sin^2 2\theta_{13}$ below 10^{-5} ! With this level of sensitivity $\nu_e \to \nu_\mu$ oscillations driven by the sub–leading δm^2 scale might be observed. The number of muon decays required to produce 10 $\nu_e \to \nu_\mu$ events in a 50 kt detector 2800 km downstream of a neutrino factory is shown for a bimaximal mixing scenario ($\sin^2 2\theta_{13} = 0$) in Fig. 12 as a function of the stored muon energy. Approaching 10^{21} muon decays might be sufficient to observe oscillations driven by the sub–leading scale.

With a vanishing or very small $\sin^2 2\theta_{13}$ only the $\nu_\mu \to \nu_\tau$ oscillations will have a significant rate, and the oscillation parameters $\sin^2 2\theta_{23}$ and δm^2_{32} can be determined by fitting the right–sign muon (ν_μ disappearance) spectrum. Good sensitivity can be obtained provided the baseline is chosen such that the first oscillation maximum occurs in the middle of the visible energy spectrum. As a first example, spectra of events tagged by right–sign muons are shown in Fig. 24 as a function of δm^2_{32} for a 10 kt MINOS–type detector 2800 km downstream of a 30 GeV neutrino factory in which there are $2 \times 10^{20}\mu^-$ decays in the beam–forming straight section. The position of the oscillation maximum (resulting in a dip in the observed distributions) is clearly sensitive to δm^2_{32}. The depth of the observed dip is sensitive to the oscillation amplitude, and hence to $\sin^2 2\theta_{23}$. The visible energy spectrum of right–sign muon events can be fit to obtain $\sin^2 2\theta_{23}$ and δm^2_{32}. We begin by considering the statistical precision that could be obtained with a perfect detector having MINOS–type resolution functions, no backgrounds, and no systematic uncertainty on the neutrino flux. Fit results are shown in Fig. 25. For $\delta m^2_{32} = 3.5 \times 10^{-3}$ eV^2/c^4 the fit yields a statistical precisions of a few percent on the the values of the oscillation parameters. If L is increased to 7332 km, the statistical precision improves to about 1%. With this level of statistical precision it is likely that systematic uncertainties will be significant. To illustrate this in Fig. 26 the 1σ contours are shown in the (δm^2_{32}, $\sin^2 2\theta_{23}$) from fits which include backgrounds together with 1% and 2% systematic uncertainties on the beam flux. With a 1% flux uncertainty the precision on δm^2_{32} and $\sin^2 2\theta_{23}$ are respectively x% and y%.

As a second example, consider a 10 kt ICANOE–type detector that is downstream of a 30 GeV neutrino factory in which there are $10^{20}\mu^+$ decays in the beam–forming straight section followed by $10^{20}\mu^-$ decays. The sensitivity to the oscillation parameters has been studied by fitting simulated visible energy distributions for events tagged by a right–sign muon. The analysis includes a 2% bin-to-bin uncorrelated systematic error on the number of neutrino interactions which takes into account the uncertainties on neutrino flux, the cross section, and the selection efficiency. To reduce background from charged meson decays, the events entering the fit are those with muons having momenta > 2 GeV. Figures 27-30 show fit results in the ($\sin^2 2\theta_{23}$, δm^2_{32})–plane as a function of the oscillation parameters and baseline. Note that for the "short" baseline (L = 732 km) the first oscillation maximum for the reference value of $\delta m^2_{32} = 3.5 \times 10^{-3}$ eV^2/c^4 occurs at a neutrino energy of about 2 GeV. This is too low to produce a clear dip in the visible energy spectrum, and as a result $\sin^2 2\theta_{23}$ and δm^2_{32} can only be determined with relatively low precision (Fig. 27), and the fit results are sensitive to systematic uncertainties on the neutrino flux. At the longer baselines (L = 2900 km and 7400 km) the oscillation dip is visible, and the oscillation parameters can be measured with a precision that is mostly determined by the statistical uncertainty (Fig. 28). For a 30 GeV neutrino factory and $\delta m^2_{32} = 3.5 \times 10^{-3}$ eV^2/c^4 the longer baseline (7400 km) yields the most precise result. Specifically, for $10^{20}\mu$ decays the statistical precisions on $\sin^2 2\theta_{23}$ and δm^2_{32} are respectively about 10% and 1%. With $10^{21}\mu$ decays the $\sin^2 2\theta_{23}$ precision improves by about a factor of 2. It should be noted that the best baseline choice depends on δm^2_{32} (Figs. 29-30), or more specifically $\delta m^2_{32}/E$.

We conclude that, within the framework of three–flavor mixing, the oscillation parameters $\sin^2 2\theta_{13}$, $\sin^2 2\theta_{23}$, and δm^2_{32} can be determined at a neutrino factory by fitting the observed visible energy distributions for various event types. A comprehensive study of the expected precisions of the measurements as a function of the oscillation parameters, baseline, and neutrino factory parameters has not yet been undertaken. However, detailed studies have been made for some examples in which there are $10^{20}\mu^+$ decays followed by $10^{20}\mu^-$ decays in a 30 GeV neutrino factory. For these examples we find that (i) if $\sin^2 2\theta_{13} > \mathrm{O}(10^{-2})$ global fits can be used to determine its value, (ii) if $\sin^2 2\theta_{13}$ is too small to observe $\nu_e \to \nu_\mu$ oscillations then we would expect to place the very stringent upper limit on its value of 10^{-3} or better, and (iii) the values of $\sin^2 2\theta_{23}$, and δm^2_{32} could be determined with precisions of respectively better than or of order 10% and of order 1%, provided the baseline is chosen so that the dip corresponding to the first oscillation maximum is in the middle of the visible energy distribution. At a high–intensity neutrino factory (for example with 10^{21} decays of 50 GeV muons) the mixing angles could be measured with a precision of a few percent, and if $\sin^2 2\theta_{13}$ is vanishingly small, the resulting upper limit could be at the $\mathrm{O}(10^{-5})$–level.

5. Search for CP violation

In the majority of the three–flavor oscillation scenarios described in section xxx CP violation is expected to be too small to produce an observable effect. Nevertheless, in these cases stringent limits on CP violation would provide an important check of the overall interpretation of the oscillation data. If however the LAM scenario provides the correct description of neutrino oscillations, CP violating effects might be sufficiently large to be observable at a high–intensity neutrino factory. This is illustrated in Fig. 31 which shows, as a function of baseline at a 20 GeV neutrino factory, the ratio R for $\delta = 0$ and $\pm\pi/2$, where R is defined as the $\overline{\nu}_e \to \overline{\nu}_\mu$ event rate divided by the $\nu_e \to \nu_\mu$ event rate. The upper group of curves is for $\delta m^2_{32} < 0$, the lower group is for $\delta m^2_{32} > 0$, and the statistical errors correspond to 10^{21} muon decays of each sign with a 50 kt detector. If L is a few thousand km a non–zero δ can produce a modification to R that is sufficiently large to be measured !

Since the $\nu_e \to \nu_\mu$ oscillation rates are to a good approximation proportional to $\sin^2 2\theta_{13}$, it is useful to define the $\sin^2 2\theta_{13}$ reach as that value of $\sin^2 2\theta_{13}$ that will produce a 3σ change in the predicted ratio R when δ is changed from 0 to $\pm\pi/2$. The $\sin^2 2\theta_{13}$ reach is shown as a function of baseline and stored muon energy in Fig. 32 for a 50 kt detector at a neutrino factory in which there are $10^{21}\mu^+$ decays followed by $10^{21}\mu^-$ decays. With an optimum baseline of about 3000 km (for $\delta m^2_{32} = 3.5 \times 10^{-3}$ eV^2/c^4) the $\sin^2 2\theta_{13}$ reach is approximately 10^{-2}, an order of magnitude below the current experimental bound. Thus, in a LAM scenario, CP violation in the lepton sector might be measurable at a neutrino factory providing $\mathrm{O}(10^{21})$ muon decays.

As an example, consider a 40 kt Fe-scintillator detector downstream of a 50 GeV neutrino factory providing $10^{21}\mu^+$ decays followed by $10^{21}\mu^-$ decays in the beam–forming straight section. The results of fits to the simulated wrong–sign muon event distributions, with δ and $\sin^2 2\theta_{13}$ left as free parameters, are shown in Fig. 33 for various baselines, with the sub–leading scale $\delta m^2_{21} = 1 \times 10^{-4}$ eV^2/c^4. The analysis includes the detector resolutions, reasonable event selection criteria, and backgrounds. As might be expected from Fig. 31 at $L = 7332$ km there is little sensitivity to δ, and at the "short" baseline $L = 732$ km the fit has difficulty untangling δ from $\sin^2 2\theta_{13}$. However, at a baseline of $L = 3500$ km for the example shown δ and $\sin^2 2\theta_{13}$ can be determined with precisions of respectively about 15° and a few percent. Note that a combination of baselines can yield a modest improvement in the precision of the measurement. The sensitivity to CP violation decreases with decreasing δm^2_{21}. Figure 34 shows as a function of $\sin^2 2\theta_{13}$ the lowest value of δm^2_{21} for which the maximal CP phase $\delta = \pi/2$ can be distinguished from a vanishing phase at $L = 3500$ km. This limiting δm^2_{21} is below the current central value for the LAM parameter space suggested by solar neutrino deficit, and is about 2×10^{-5} eV^2/c^4, independent of $\sin^2 2\theta_{13}$.

E. Summary

The oscillation physics that could be pursued at a neutrino factory appears to be compelling. In particular, experiments at a neutrino factory would be able to simultaneously measure, or put stringent limits on, all of the appearance modes $\nu_e \to \nu_\tau$, $\nu_e \to \nu_\mu$, and $\nu_\mu \to \nu_\tau$. Comparing the sum of the appearance modes with the disappearance measurements would provide a unique basic check of the candidate oscillation scenario that cannot be made with a conventional neutrino beam. In addition, for all of the specific oscillation scenarios we have studied, the ν_e component in the beam can be exploited to enable crucial physics questions to be addressed. These include (i) the pattern of neutrino masses (sign of δm^2), (ii) the precise determination of (or stringent limits on) all of the leading oscillation parameters, which in a three–flavor mixing scenario would be $\sin^2 2\theta_{13}$, $\sin^2 2\theta_{23}$, and δm^2_{32}, and (iii) the observation of, or stringent limits on, CP violation in the lepton sector, and a corresponding measurement of the phase δ.

To be more quantitative in assessing the beam energy, intensity, and baseline required to accomplish a given set of physics goals it is necessary to consider two very different experimental possibilities: (a) the LSND oscillation results are confirmed by the MiniBooNE experiment, or (b) they are not confirmed.

(a) LSND not confirmed. Fairly extensive neutrino factory studies have been made within the framework of three–flavor oscillation scenarios in which there is one "large" δm^2 scale identified with the atmospheric neutrino deficit results, and one small δm^2 identified with the solar neutrino deficit results. A summary of the energy dependent beam intensities required to cross a variety of "thresholds of interest" is provided by Fig. 12. A 20 GeV neutrino factory providing 10^{19} muon decays per year is a good candidate "entry–level" facility which would enable either (i) the first observation of $\nu_e \to \nu_\mu$ oscillations, the first direct measurement of matter effects, and a determination of the sign of δm^2_{32} and hence the pattern of neutrino masses, or (ii) a very stringent limit on $\sin^2 2\theta_{13}$ and a first comparison of the sum of all appearance modes with the disappearance measurements. The optimum baseline for this entry–level physics program appears to be of order 3000 km, for which both matter effects and event rates are substantial. A 20 GeV neutrino factory providing 10^{20} muon decays per year is a good candidate upgraded neutrino factory (or alternatively a higher energy facility providing a few $\times 10^{19}$ decays per year). This would enable the first observation of, or meaningful limits on, $\nu_e \to \nu_\tau$ oscillations, and precision measurements of the leading oscillation parameters. In the more distant future, a candidate for a second (third ?) generation neutrino factory might be a facility that provides O(10^{21}) decays per year and enables the measurement of, or stringent limits on, CP violation in the lepton sector.

(b) LSND confirmed. Less extensive studies have been made for the class of scenarios that become of interest if the LSND oscillation results are confirmed. However, in the scenarios we have looked at (IB1 and IC1) we find that the $\nu_e \to \nu_\tau$ rate is sensitive to the oscillation parameters and can be substantial. With a large leading δm^2 scale medium baselines (for example a few $\times 10$ km) are of interest, and the neutrino factory intensity required to effectively exploit the ν_e beam component might be quite modest ($< 10^{19}$ decays per year).

General comments about what we have and have not done. Comments about polarization.

REFERENCES

[1] R. Forty, JHEP 9912:002,1999 `hep-ex/9910061`

[2] need other geer reference with muon energy cut...plus V. Barger, S. Geer, R. Raja, K. Whisnant, `hep-ph/9911524`

[3] P. Strolin, Nufact'99 Workshop,July 5-9th, Lyon

[4] D.A. Harris, A. Para, `hep-ex/0001035`

[5] W.W. Armstrong *et al*, Atlas Technical Proposal.

[6] D.A. Harris, J.Yu *et al.*, NuTeV collaboration, hep-ex/9908056. *To appear in Nucl.Instrum.Meth.A.*

[7] Numonte Reference...TBA

[8] Doke, *et al.*, Nucl. Instrum. Meth **A237** 475 (1985)

[9] A. Cervera et al., "Golden measurements at a neutrino factory", hep-ph/0002108.

[10] V. Barger, S. Geer, R. Raja, K. Whisnant, "Neutrino oscillations at an entry–level neutrino factory and beyond", Fermilab-PUB 00/049-T.

[11] M. Campanelli et al., in preparation.

[12] R. Bernstein, in preparation.

TABLE III. Wrong-sign muon rates for a 50 kt detector (with a muon threshold of 4 GeV) a distance L downstream pf a muon factory (energy E_μ) providing 10^{19} muon decays. Rates are shown for LAM scenario IA1 with both signs of δm^2_{32} considered separately. The background rates listed correspond to an assumed background level of 10^{-4} times the total CC rates. Results are from Ref. xxxx

E_μ	L	μ^+ stored			μ^- stored		
GeV	km	$\delta m^2_{32} > 0$	$\delta m^2_{32} < 0$	Backg	$\delta m^2_{32} > 0$	$\delta m^2_{32} < 0$	Backg
20	732	52.	36.	7.3	32.	26.	6.5
	2800	46.	9.2	0.43	7.1	26.	0.36
	7332	33.	0.97	0.063	0.55	19.	0.05
30	732	100.	72.	25.	58.	45.	24.
	2800	90.	26.	1.6	19.	43.	1.4
	7332	43.	3.3	0.19	2.1	33.	0.17
40	732	150.	110.	60.	83.	65.	58.
	2800	140.	48.	4.0	36.	64.	3.8
	7332	54.	5.6	0.49	3.1	28.	0.43
50	732	200.	140.	120.	110.	84.	120.
	2800	180.	71.	7.9	53.	82.	7.7
	7332	56.	8.0	1.1	5.0	34.	1.0

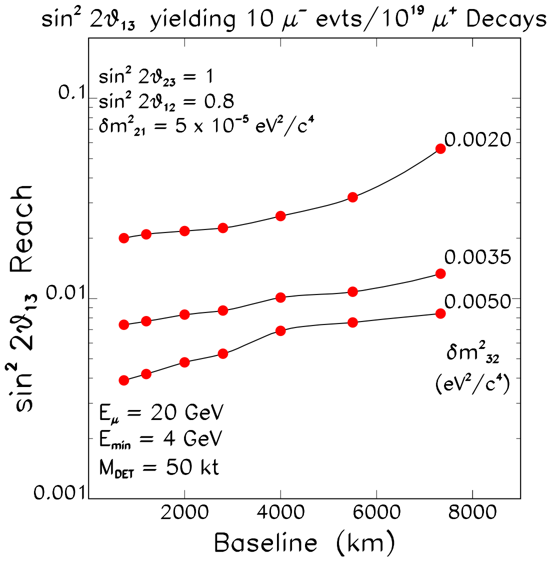

FIG. 11. Reach in $\sin^2 2\theta_{13}$ for the observation of 10 μ^- events from $\nu_e \to \nu_\mu$ oscillations, shown versus baseline for three δm^2_{32} spanning the favored SuperK range. The other oscillation parameters correspond to the LAM scenario IA1. The curves correspond to $10^{19}\mu^+$ decays in a 20 GeV neutrino factory with a 50 kt detector, and a minimum muon detection threshold of 4 GeV. Result are from Ref. xxx.

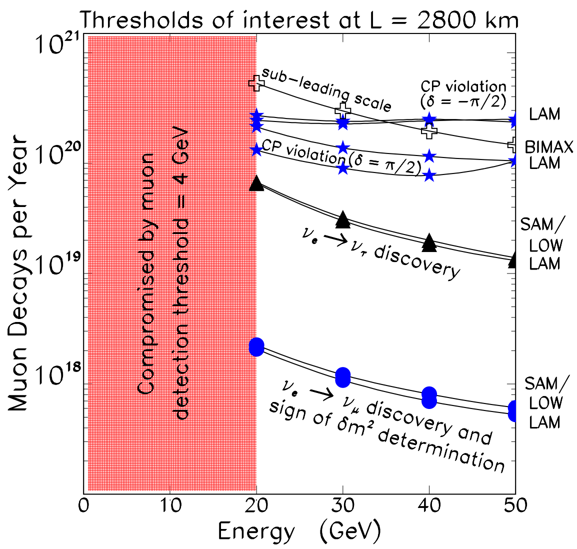

FIG. 12. The required number of muon decays needed in the beam–forming straight section of a neutrino factory to achieve the physics goals described in the text, shown as a function of storage ring energy for the LAM scenario IA1, SAM scenario IA2, LOW scenario IA3, and a bimaximal mixing scenario BIMAX. The baseline is taken to be 2800 km, and the detector is assumed to be a 50 kt wrong–sign muon appearance device with a muon detection threshold of 4 GeV or, for $\nu_e \to \nu_\tau$ appearance, a 5 kt detector. Result are from Ref. xxx.

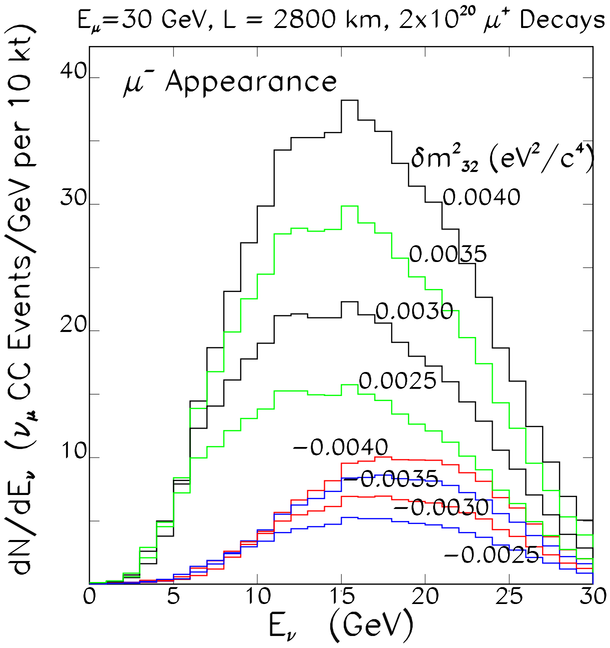

FIG. 13. Predicted measured energy distributions for CC events tagged by a wrong-sign (negative) muon from $\nu_e \to \nu_\mu$ oscillations, shown for various δm^2_{32}, as labeled. The predictions correspond to 2×10^{20} decays, $E_\mu = 30$ GeV, $L = 2800$ km, with the values for δm^2_{12}, $\sin^2 2\theta_{13}$, $\sin^2 2\theta_{23}$, $\sin^2 2\theta_{12}$, and δ corresponding to the LAM scenario IA1. Result are from Ref. xxx.

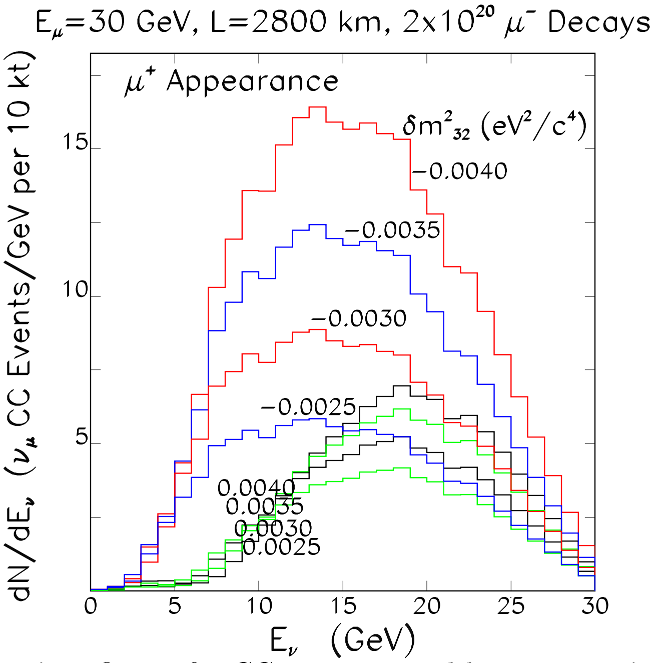

FIG. 14. Same as previous figure, for CC events tagged by a wrong-sign (positive) muon from $\bar{\nu}_e \to \bar{\nu}_\mu$ oscillations.

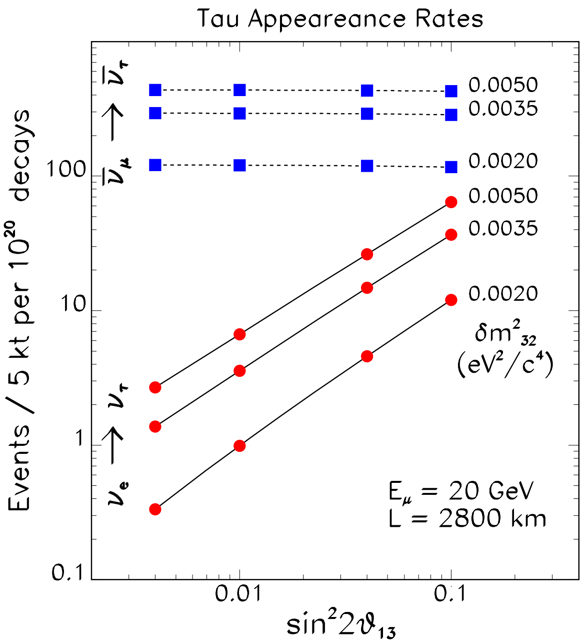

FIG. 15. ν_τ CC appearance rates in a 5 kt detector 2800 km downstream of a 20 GeV neutrino factory in which there are $10^{20}\mu^+$ decays in the beam–forming straight section. The rates are shown as a function of $\sin^2 2\theta_{13}$ and δm^2_{32} with the other oscillation parameters corresponding to the LAM scenario IA1. The top 3 curves are the predictions for $\overline{\nu}_\mu \rightarrow \overline{\nu}_\tau$ events and the lower curves are for $\nu_e \rightarrow \nu_\tau$ events. Result are from Ref. xxx.

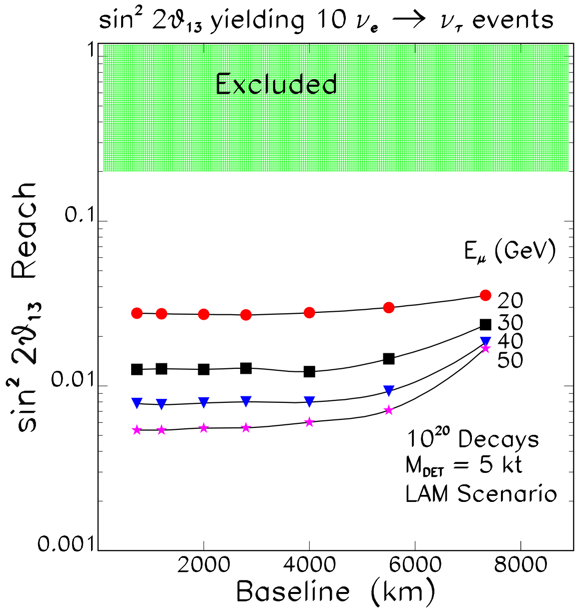

FIG. 16. Reach in $\sin^2 2\theta_{13}$ for the observation of 10 $\nu_e \rightarrow \nu_\tau$ oscillation events, shown as a function of baseline for four storage ring energies. The oscillation parameters correspond to the LAM scenario IA1. The curves correspond to 10^{20} μ^+ decays in a 20 GeV neutrino factory with a 5 kt detector. Result are from Ref. xxx.

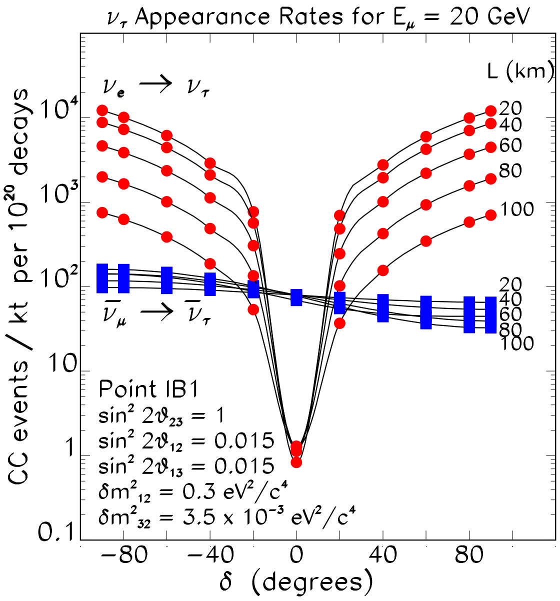

FIG. 17. ν_τ CC appearance rates in a 1 kt detector downstream of a 20 GeV neutrino factory in which there are $10^{20}\mu^+$ decays. Rates are shown as a function of the baseline L and phase δ, with the other oscillation parameters corresponding to the LSND + Atmospheric scenario IB1. Predictions for $\nu_e \to \nu_\tau$ and $\overline{\nu}_\mu \to \overline{\nu}_\tau$ are shown separately, as labeled. Result are from Ref. xxx.

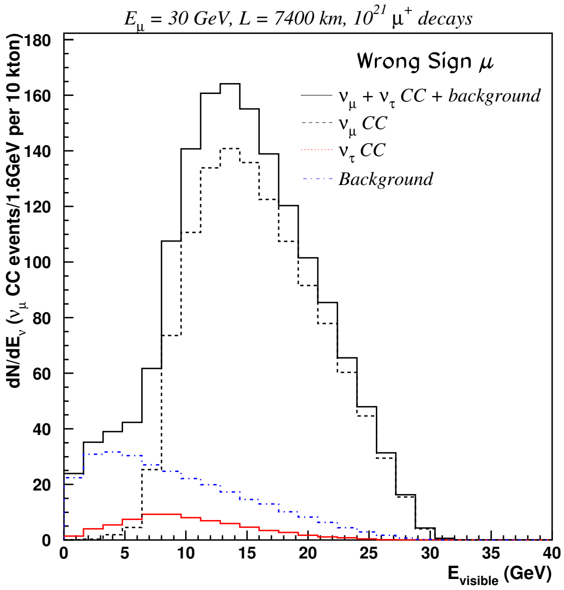

FIG. 18. Visible energy spectrum for events tagged by wrong-sign muons in an ICANOE–type detector (full histogram). The oscillation parameters are $\delta m^2_{32} = 3.5 \times 10^{-3}$ eV^2/c^4, $\sin^2\theta_{23} = 1$, and $\sin^2 2\theta_{13} = 0.05$. Also shown are the contributions from $\nu_e \to \nu_\mu$ oscillations (black dashed curve), $\nu_e \to \nu_\tau$, with a subsequent muonic decay of the τ lepton (red curve), and background from muonic decays of pions or kaons in neutral current or charged current events (blue dot-dashed curve). Result are from Ref. xxx.

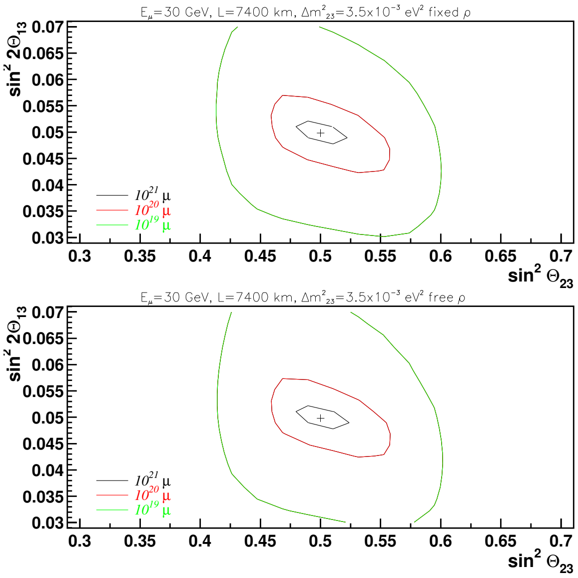

FIG. 19. Results from a global fit to the visible energy distributions for various event classes recorded in a 10 kt ICANOE–type detector 7400 km downstream of a 30 GeV neutrino factory. The 68% CL contours correspond to experiments in which there are 10^{19}, 10^{20}, and $10^{21}\mu^+$ decays in the neutrino factory (as labelled) followed by the same number of μ^- decays. Upper plot: density fixed to its true value. Lower plot: density is a free parameter of the fit. Result are from Ref. xxx.

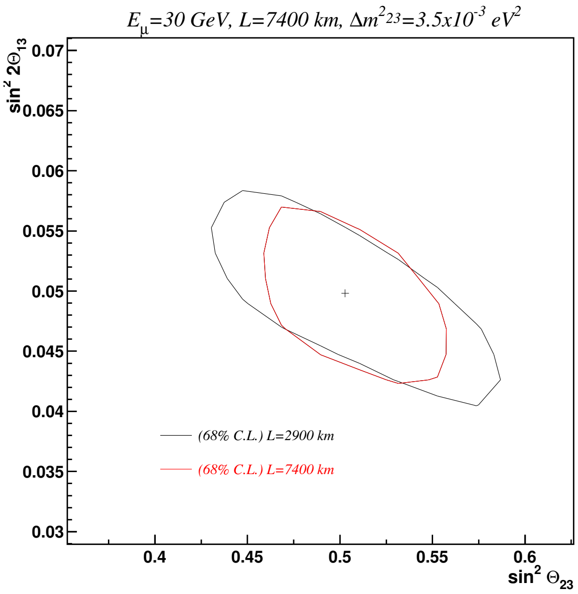

FIG. 20. Results from a global fit to the visible energy distributions for various event classes recorded in a 10 kt ICANOE–type detector downstream of a 30 GeV neutrino factory in which there are $10^{20}\mu^+$ decays in the neutrino factory followed by the same number of μ^- decays. The 68% CL contours correspond to baselines of 7400 km and 2900 km, as labelled. Result are from Ref. xxx.

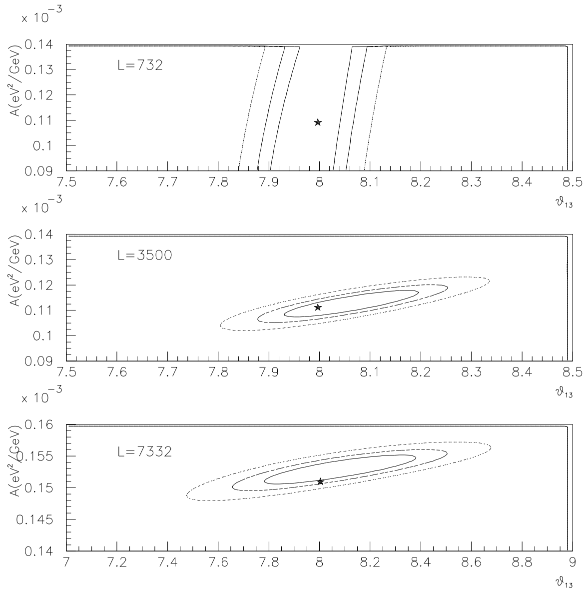

FIG. 21. Fit results in the (density parameter, θ_{13})–plane for a simulated experiment in which a 40 kt Fe-scintillator detector is a distance L km downstream of a 50 GeV neutrino factory in which there are $10^{21}\mu$ decays. The curves are 68.5, 90, and 99% CL contours. Result are from Ref. xxx.

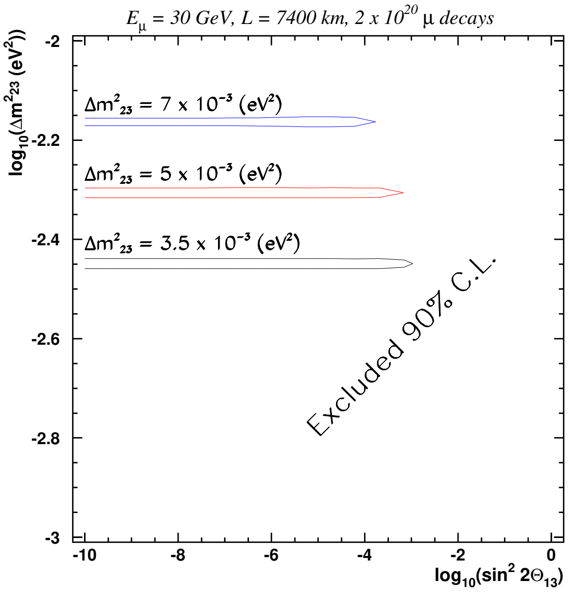

FIG. 22. Allowed regions in oscillation parameter space calculated for a simulated experiment in which $10^{20}\mu^+$ followed by $10^{20}\mu^-$ decay in a 30 GeV neutrino factory that is 7400 km from a 10 kt ICANOE–type detector. This result is two orders of magnitude better than the analogous for ICANOE at the CNGS. Result are from Ref. xxx.

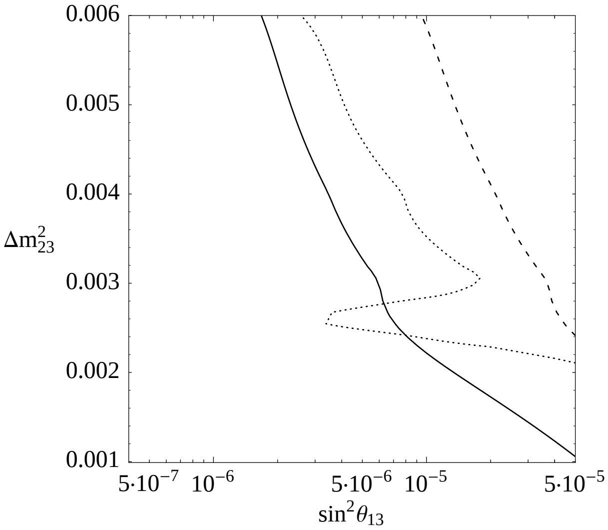

FIG. 23. Allowed regions in oscillation parameter space calculated for a simulated experiment in which a 40 kt Fe-scintillator detector is a distance L km downstream of a 50 GeV neutrino factory in which there are $10^{21}\mu$ decays. The curves are 90% CL contours for $L = 732$ km (dashed), 3500 km (solid), and 7332 km (dotted). Result are from Ref. xxx.

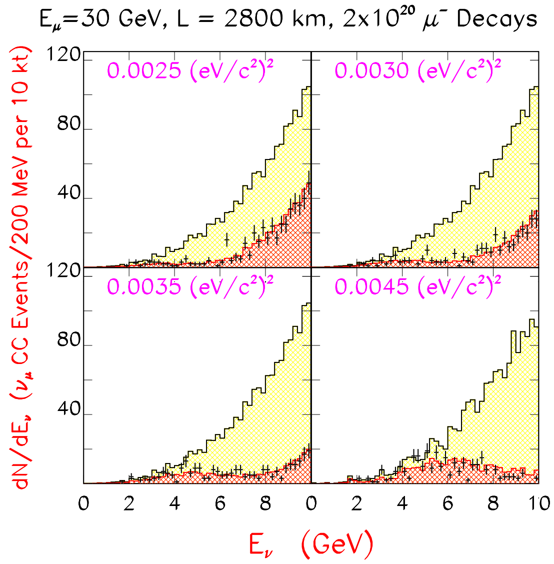

FIG. 24. Visible energy distributions for events tagged by a right–sign muon in a MINOS–type detector 2800 km downstream of a 20 GeV neutrino factory in which there are $2 \times 10^{20}\mu^-$ decays. Predicted distributions are shown for four values of δm^2_{32}, with the other parameters corresponding to the LAM scenario IA1. For each panel, the points with statistical error bars show an example of a simulated experiment. The light shaded histograms show the predicted distributions in the absence of oscillations. Results are from Ref. xxx

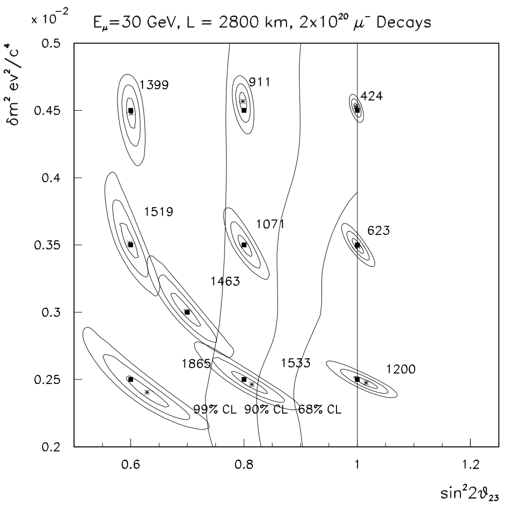

FIG. 25. Fit results for simulated ν_μ disappearance measurements with a 10 kt MINOS-type detector 2800 km downstream of a 30 GeV neutrino factory in which there are $2 \times 10^{20} \mu^-$ decays. For each trial point the 1σ, 2σ, and 3σ contours are shown for a perfect detector (no backgrounds) and no systematic uncertainty on the beam flux. The 68%, 90% and 95% SuperK regions are indicated. Result are from Ref. xxx.

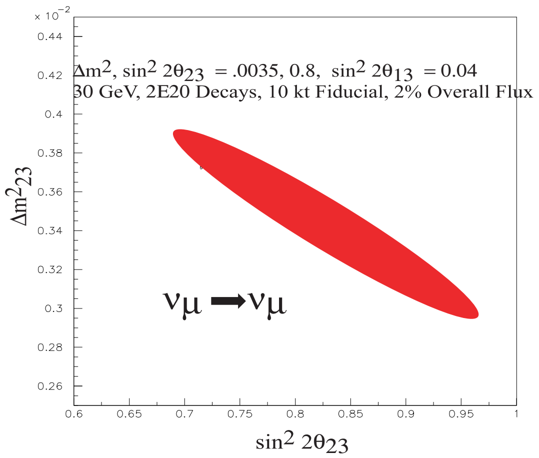

FIG. 26. Fit results (1 σ contour for simulated ν_μ disappearance measurements with a 10 kt MINOS-type detector 2800 km downstream of a 30 GeV neutrino factory in which there are $2 \times 10^{20} \mu^-$ decays. For each trial point the 1σ, 2σ, and 3σ contours are shown. Backgrounds, cuts, and a 2% systematic uncertainty on the flux are included. Result are from Ref. xxx.

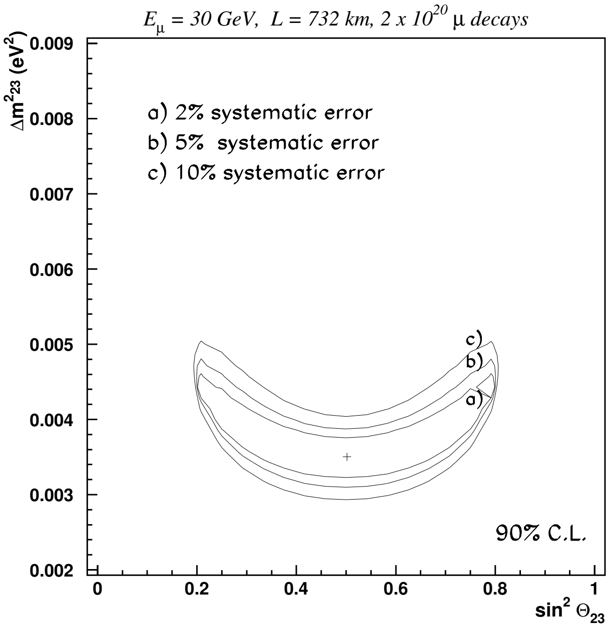

FIG. 27. Fit results for simulated ν_μ disappearance measurements with a 10 kt ICANOE type detector 732 km downstream of a 30 GeV neutrino factory in which there are $10^{20}\mu$ decays. The effect of a systematic uncertainty on the neutrino flux is shown. Result are from Ref. xxx.

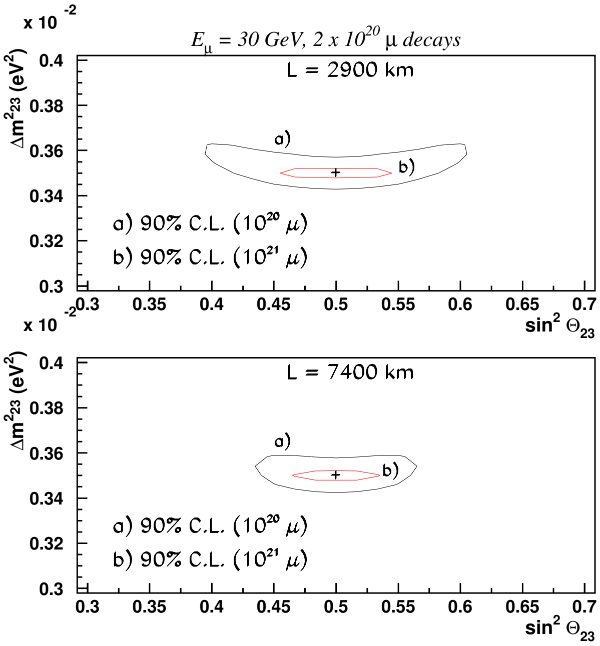

FIG. 28. Fit results for simulated ν_μ disappearance measurements with a 10 kt ICANOE type detector 2900 km (top plot) and 7400 km (bottom plot) downstream of a 30 GeV neutrino factory in which there are (a) $10^{20}\mu$ decays and (b) $10^{21}\mu$ decays. Result are from Ref. xxx.

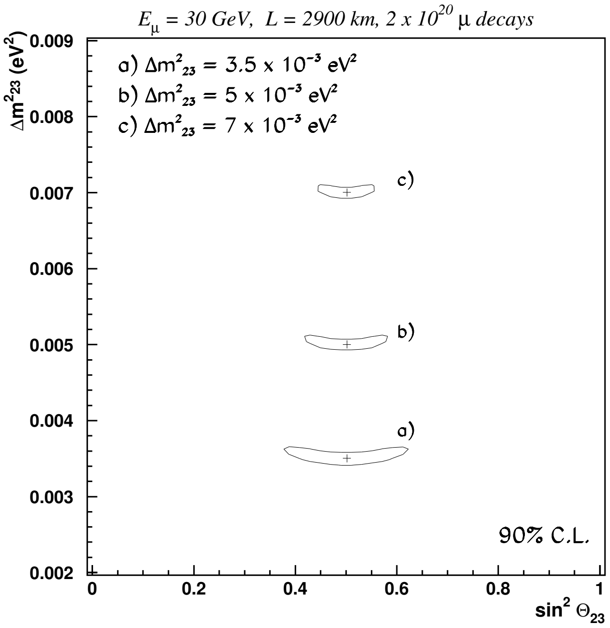

FIG. 29. Fit results for simulated ν_μ disappearance measurements with a 10 kt ICANOE type detector 2900 km downstream of a 30 GeV neutrino factory in which there are $10^{20}\mu^+$ decays followed by $10^{20}\mu^+$ decays. Result are shown for 3 values of δm^2_{32}, and are from Ref. xxx.

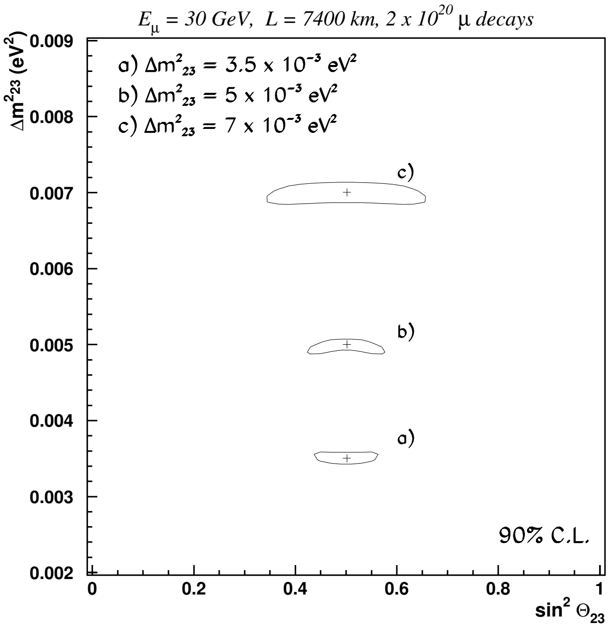

FIG. 30. Fit results for simulated ν_μ disappearance measurements with a 10 kt ICANOE type detector 7400 km downstream of a 30 GeV neutrino factory in which there are $10^{20}\mu^+$ decays followed by $10^{20}\mu^+$ decays. Result are shown for 3 values of δm^2_{32}, and are from Ref. xxx.

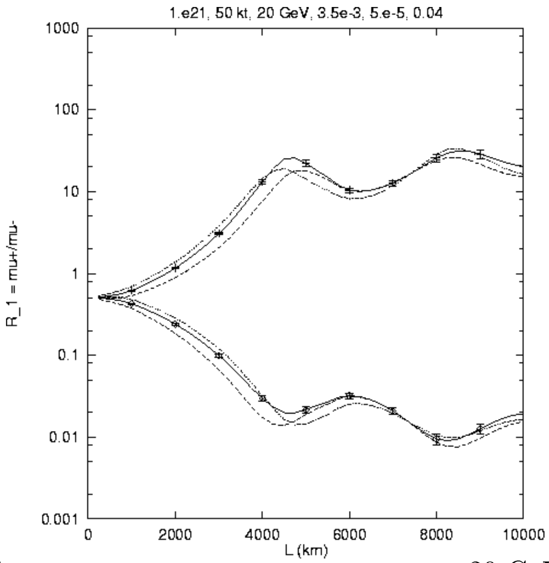

FIG. 31. The ratio R of $\bar{\nu}_e \to \bar{\nu}_\mu$ to $\nu_e \to \nu_\mu$ event rates at a 20 GeV neutrino factory for $\delta = 0$ and $\pm\pi/2$. The upper group of curves is for $\delta m^2_{32} < 0$, the lower group is for $\delta m^2_{32} > 0$, and the statistical errors correspond to 10^{21} muon decays of each sign and a 50 kt detector. The oscillation parameters correspond to the LAM scenario IA1. Result are from Ref. xxx.

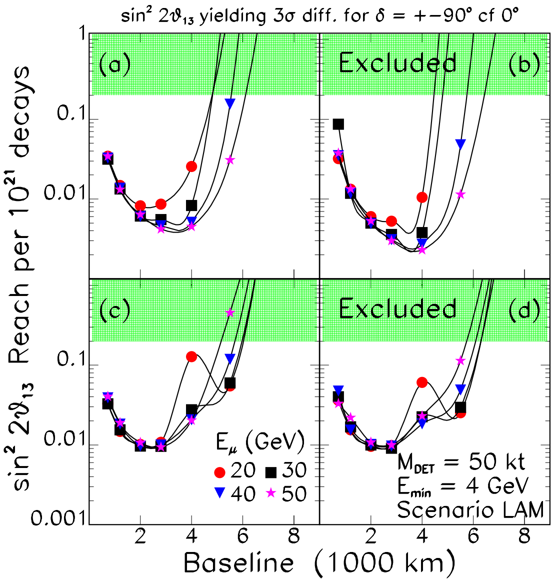

FIG. 32. Reach in $\sin^2 2\theta_{13}$ that yields a 3σ discrimination between (a) $\delta = 0$ and $\pi/2$ with $\delta m^2_{32} > 0$, (b) $\delta = 0$ and $\pi/2$ with $\delta m^2_{32} < 0$, (c) $\delta = 0$ and $-\pi/2$ with $\delta m^2_{32} > 0$, and (d) $\delta = 0$ and $-\pi/2$ with $\delta m^2_{32} < 0$. The discrimination is based on a comparison of wrong–sign muon CC event rates in a 50 kt detector when 10^{21} positive and negative muons alternately decay in the neutrino factory. The reach is shown versus baseline for four storage ring energies. The oscillation parameters correspond to the LAM scenario IA1. Result are from Ref. xxx.

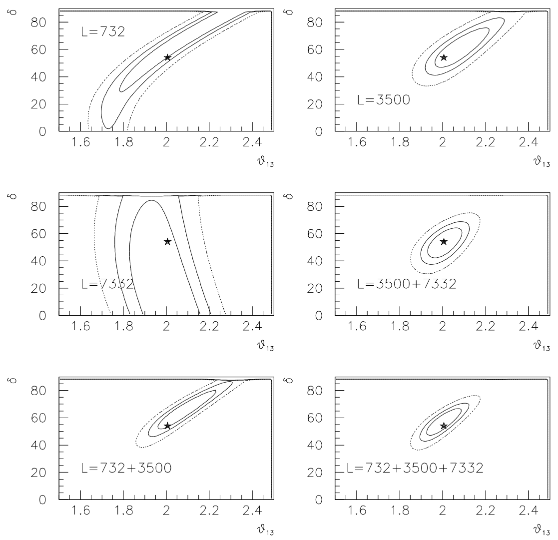

FIG. 33. Fit results in the CP phase δ versus θ_{13} plane for a LMA scenario with $\delta m^2_{21} = 1 \times 10^{-4}$ eV^2/c^4. The 68.5, 90, and 99% CL contours are shown for a 40 kt detector a distance L km downstream of a 50 GeV neutrino factory in which there are $10^{21}\mu^+$ and $10^{21}\mu^-$ decays. Result are from Ref. xxx.

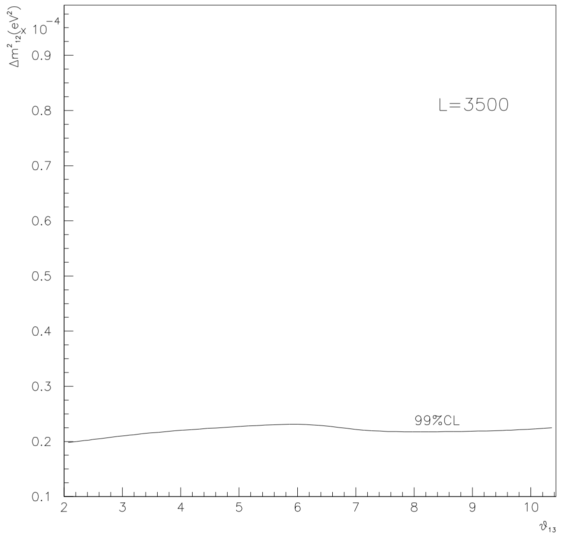

FIG. 34. The lowest value of δm^2_{21}, shown as a function of θ_{13}, for which the maximal CP phase $\delta = \pi/2$ can be distinguished from a vanishing phase in a LMA oscillation scenario. The curve corresponds to a 40 kt detector 3500 km downstream of a 50 GeV neutrino factory in which there are $10^{21}\mu^+$ and $10^{21}\mu^-$ decays. Result are from Ref. xxx.